

US007709124B2

(12) **United States Patent**
Barnett et al.

(10) **Patent No.:** **US 7,709,124 B2**
(45) **Date of Patent:** ***May 4, 2010**

(54) **DIRECT HYDROCARBON FUEL CELLS**

(56) **References Cited**

(75) Inventors: **Scott A. Barnett**, Evanston, IL (US);
Tammy Lai, Evanston, IL (US); **Jiang**
Liu, Evanston, IL (US)

(73) Assignee: **Northwestern University**, Evanston, IL
(US)

(*) Notice: Subject to any disclaimer, the term of this
patent is extended or adjusted under 35
U.S.C. 154(b) by 0 days.

This patent is subject to a terminal dis-
claimer.

(21) Appl. No.: **10/427,707**

(22) Filed: **May 1, 2003**

(65) **Prior Publication Data**

US 2004/0033405 A1 Feb. 19, 2004

Related U.S. Application Data

(63) Continuation-in-part of application No. PCT/US02/
11050, filed on Apr. 9, 2002, and a continuation-in-part
of application No. 09/833,209, filed on Apr. 10, 2001,
now Pat. No. 6,479,178.

(51) **Int. Cl.**

H01M 8/10 (2006.01)

H01M 2/00 (2006.01)

H01M 2/02 (2006.01)

H01M 2/14 (2006.01)

(52) **U.S. Cl.** **429/32; 429/34; 429/38**

(58) **Field of Classification Search** **429/34,**
429/38, 39, 32

See application file for complete search history.

U.S. PATENT DOCUMENTS

4,894,297 A	1/1990	Singh et al.	
5,273,837 A *	12/1993	Aitken et al.	429/30
5,312,700 A *	5/1994	Ishida	429/30
5,397,657 A	3/1995	Ito et al.	
5,486,428 A	1/1996	Gardner et al.	
5,516,597 A	5/1996	Singh et al.	
5,554,454 A	9/1996	Gardner et al.	
5,595,833 A	1/1997	Gardner et al.	

(Continued)

FOREIGN PATENT DOCUMENTS

EP 0275356 7/1988

(Continued)

OTHER PUBLICATIONS

Lai, Liu and Barnett, "Patterned Series-Connected Solid Oxide Fuel
Cell Arrays"; Materials Science and Engineering Department, North-
western University, Power Point Presentation, May 2003.

(Continued)

Primary Examiner—Patrick Ryan

Assistant Examiner—Julian Mercado

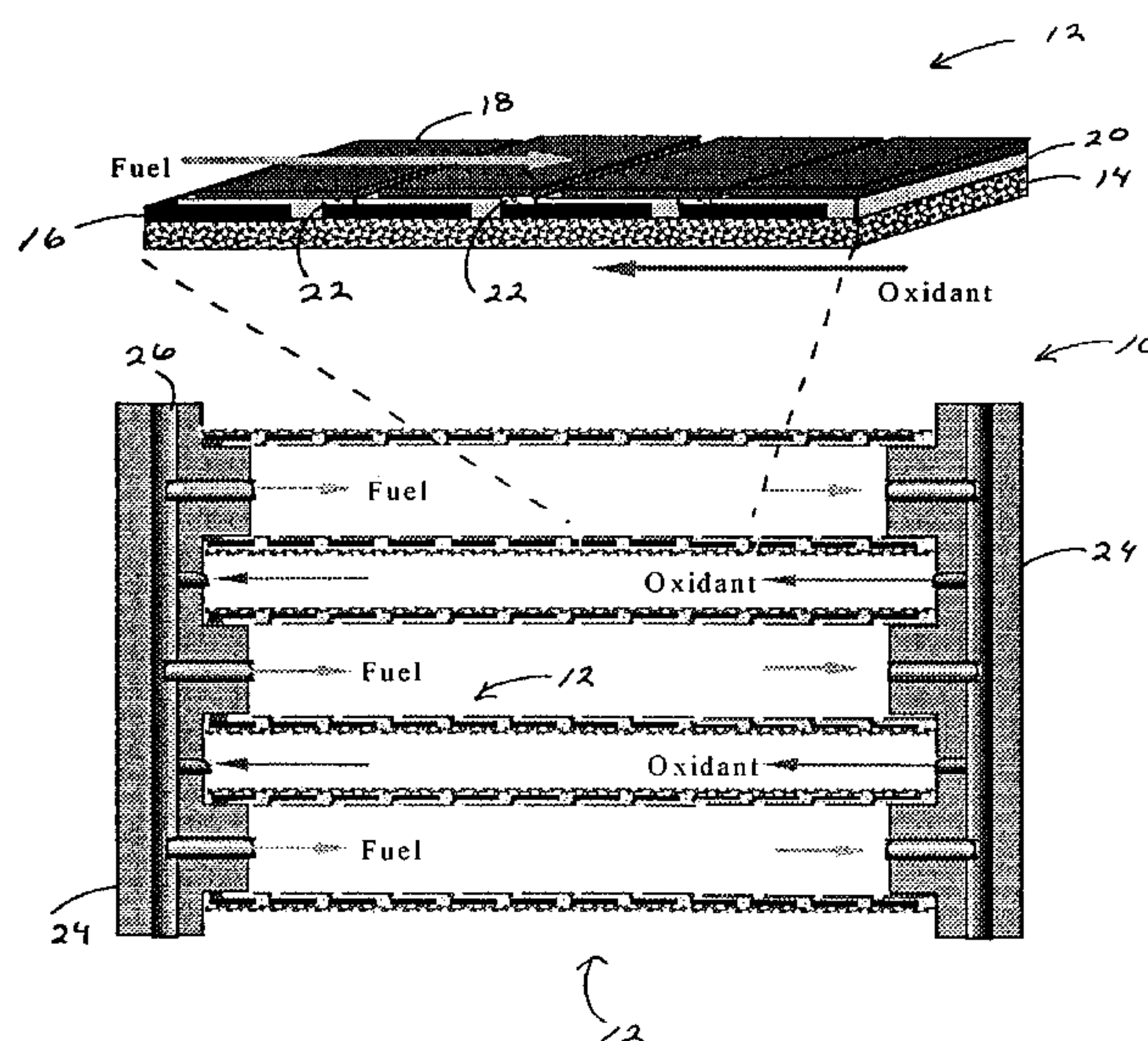
(74) *Attorney, Agent, or Firm*—Reinhart Boemer Van Deuren
S.C.

(57)

ABSTRACT

The direct electrochemical oxidation of hydrocarbons in solid
oxide fuel cells, to generate greater power densities at lower
temperatures without carbon deposition. The performance
obtained is comparable to that of fuel cells used for hydrogen,
and is achieved by using novel anode composites at low
operating temperatures. Such solid oxide fuel cells, regard-
less of fuel source or operation, can be configured advanta-
geously using the structural geometries of this invention.

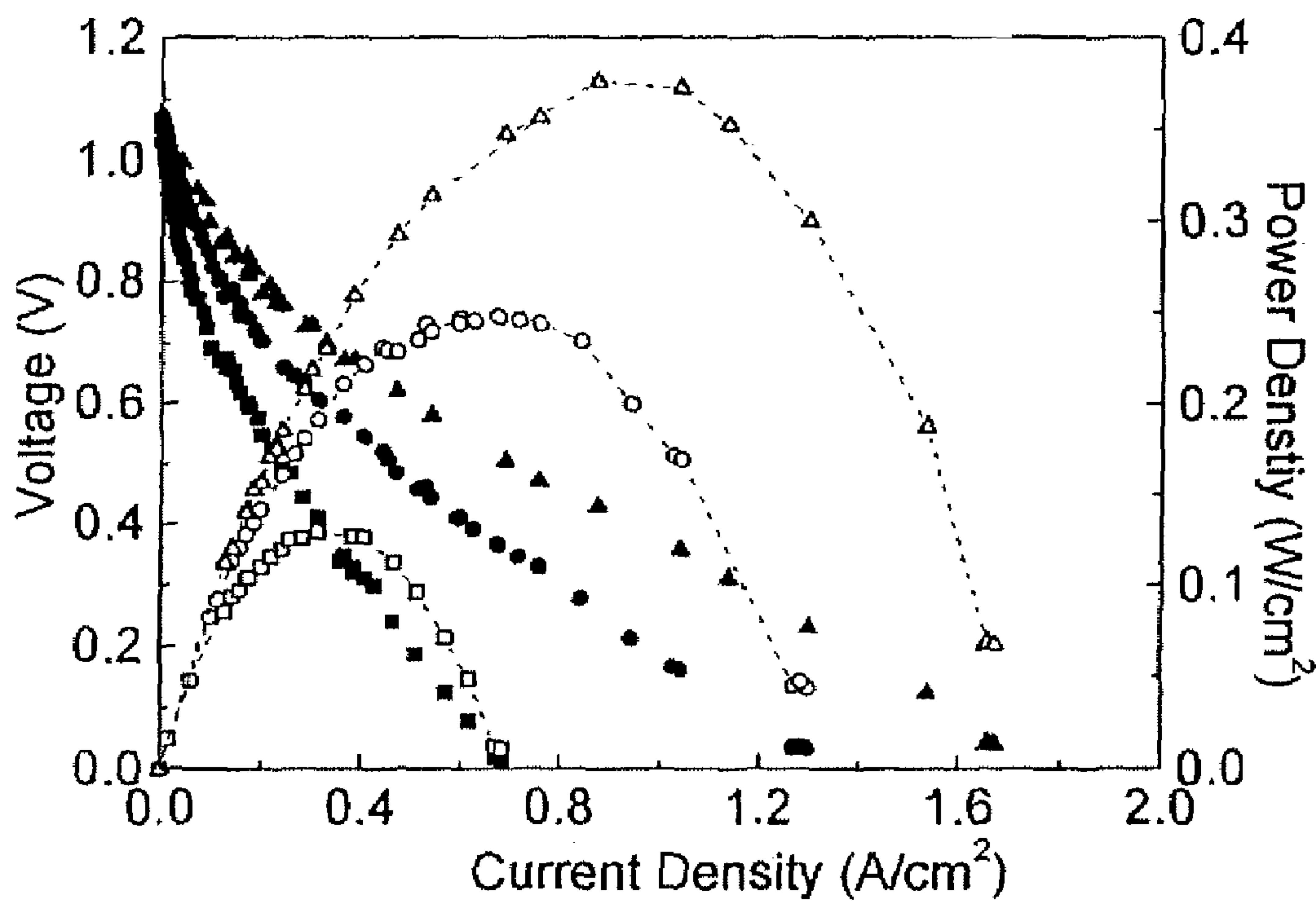
15 Claims, 27 Drawing Sheets



Page 2

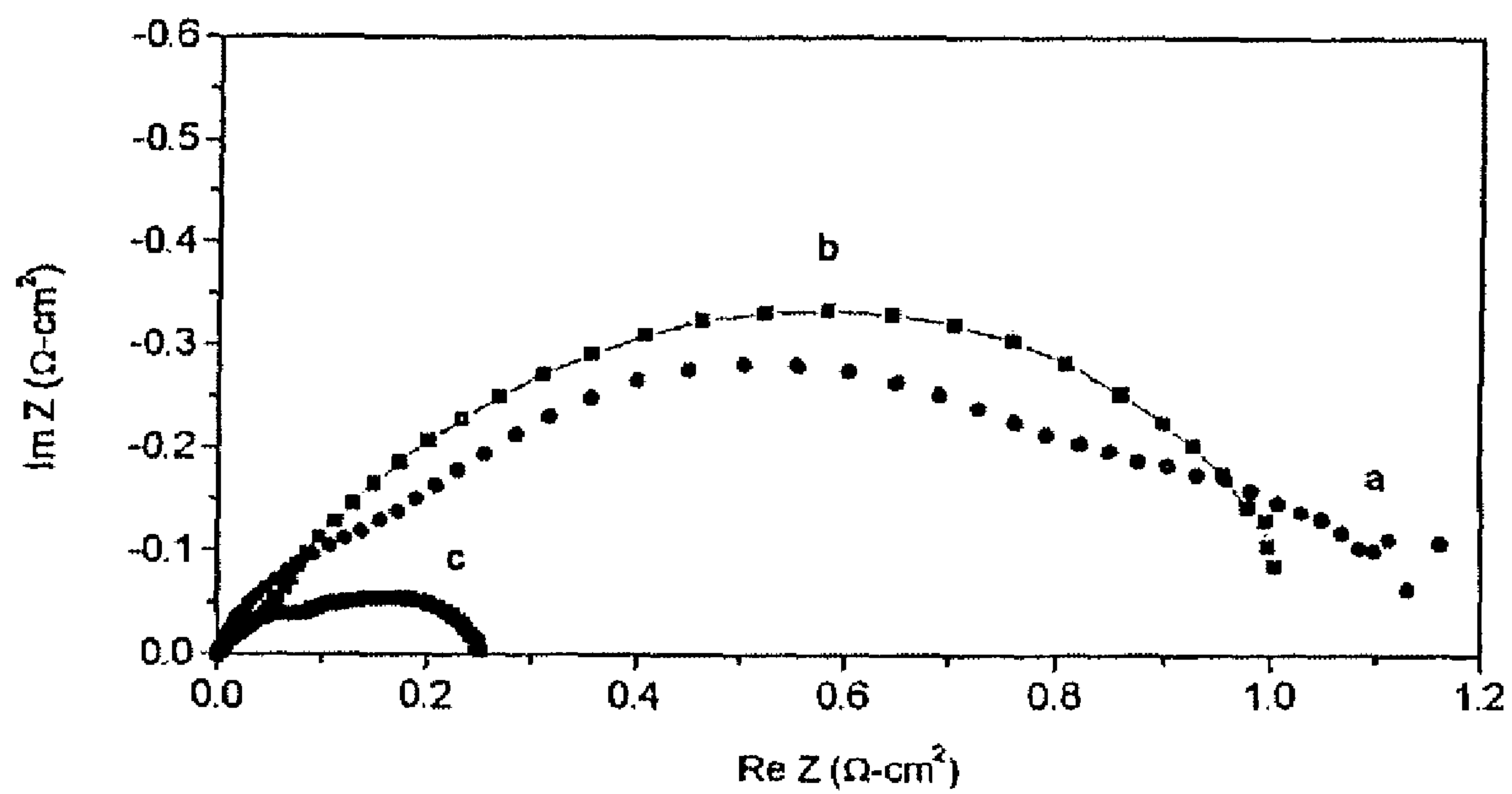
* cited by examiner

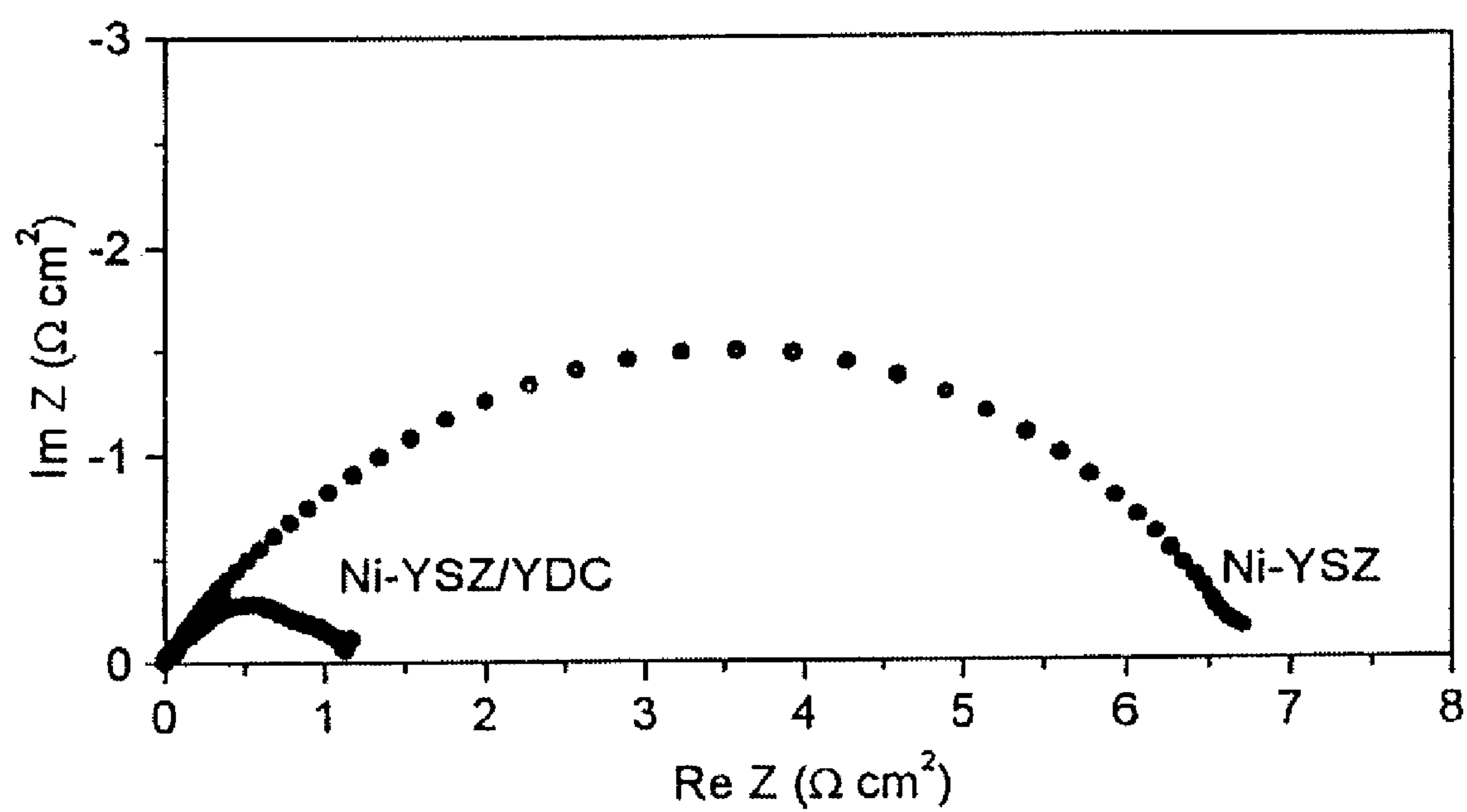
FIGURE 1A

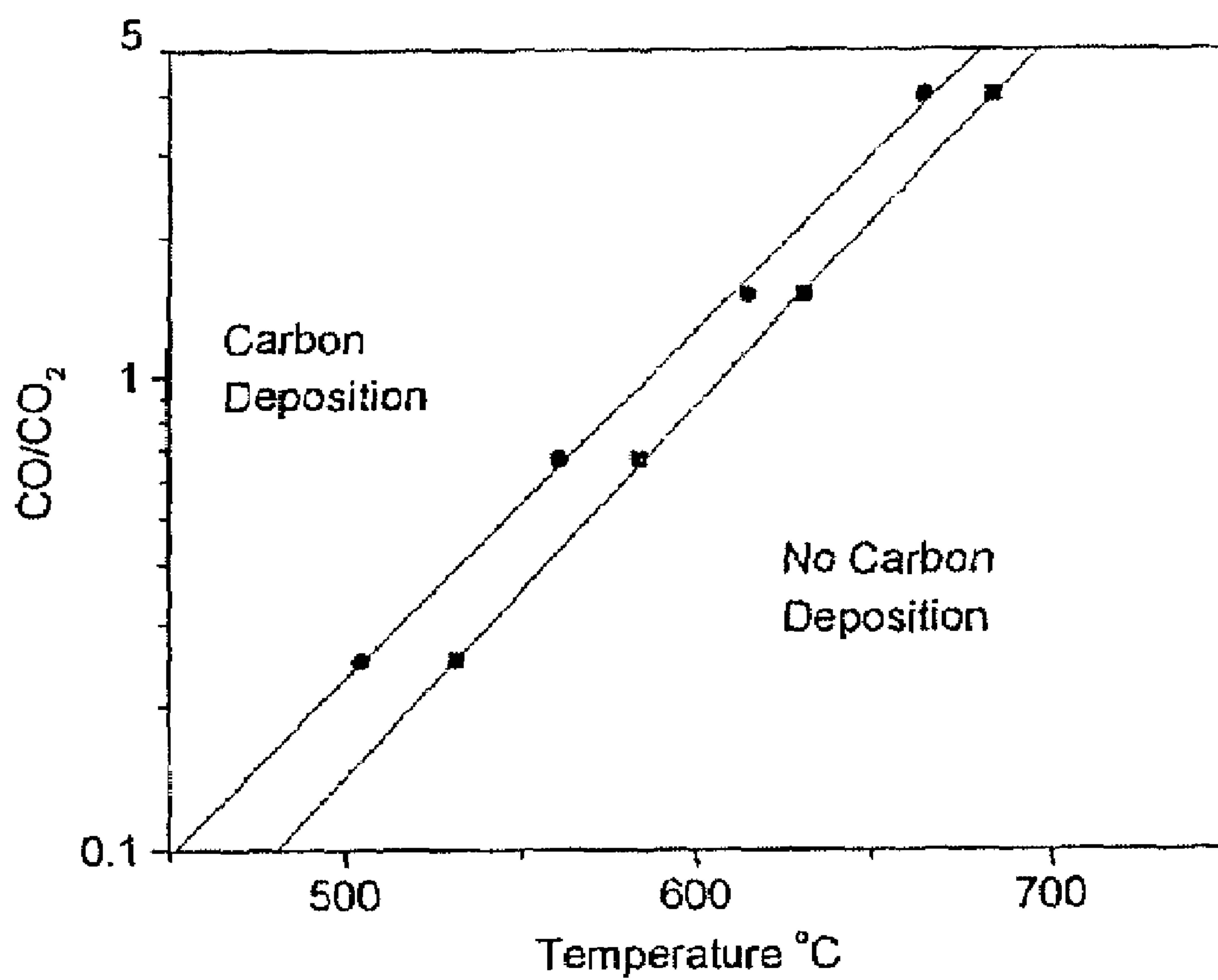


Temperature (°C)	550	600	650
Voltage (V)	■	●	▲
Power Density (W/cm ²)	□	○	△

FIGURE 1B

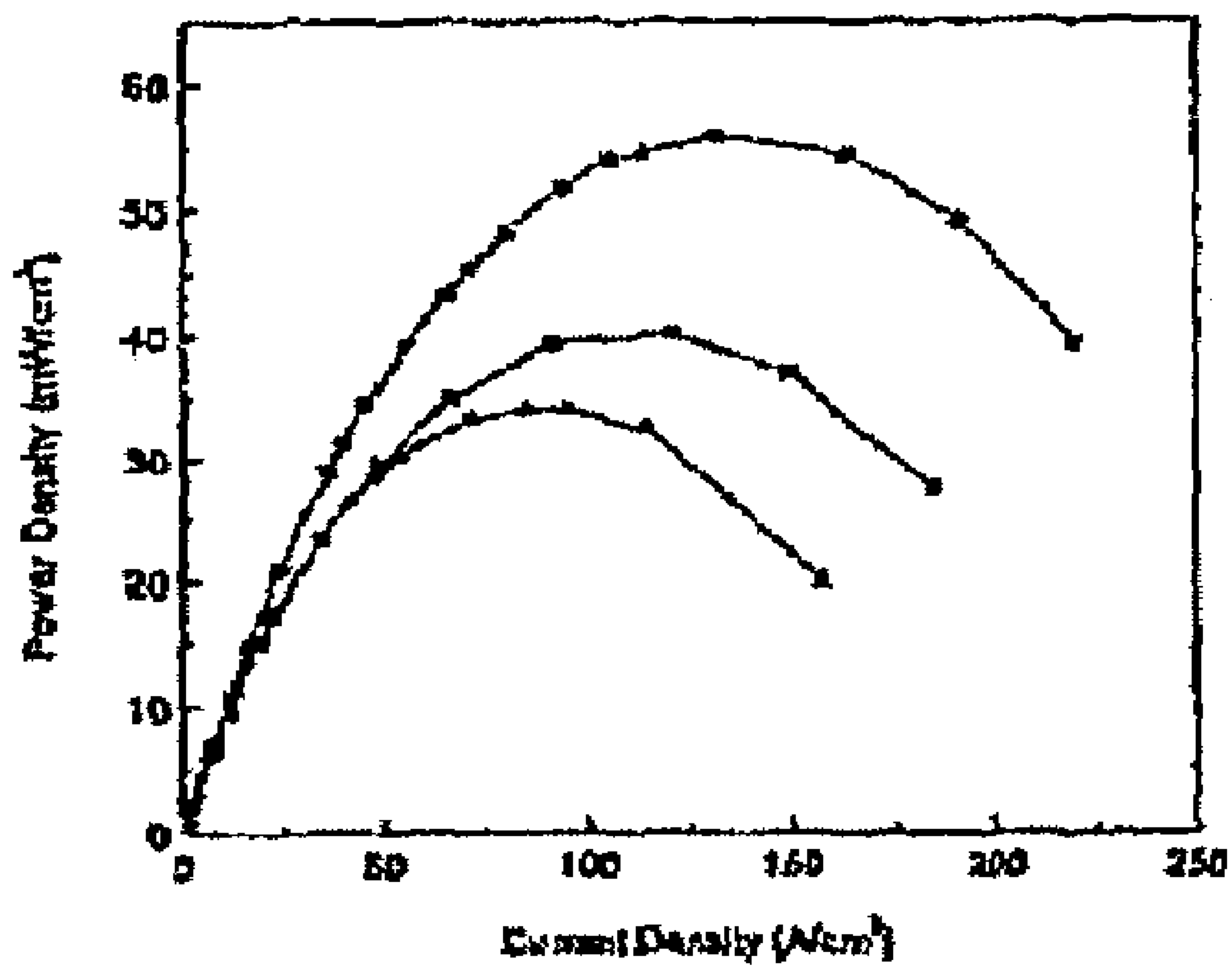
**FIGURE 2**

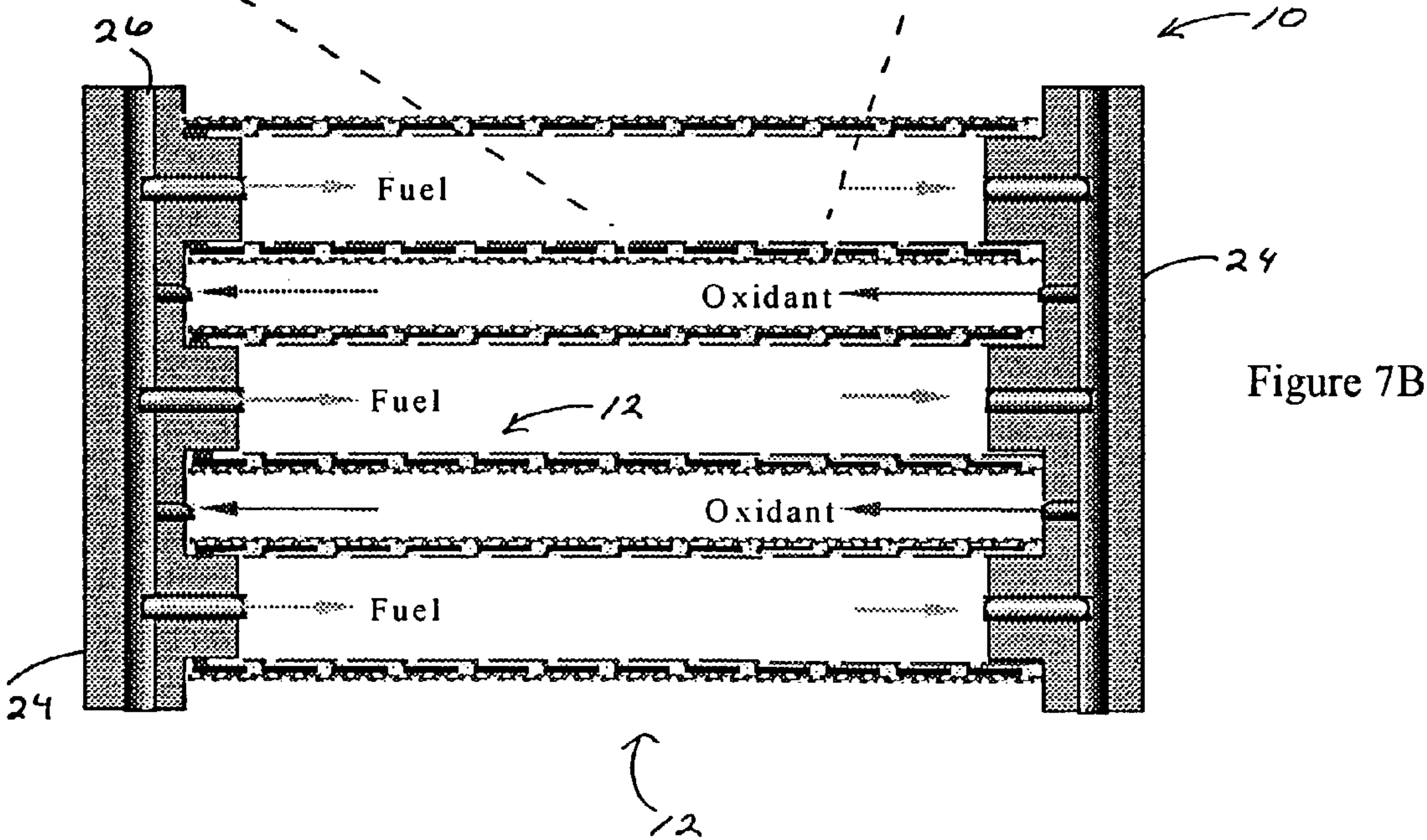
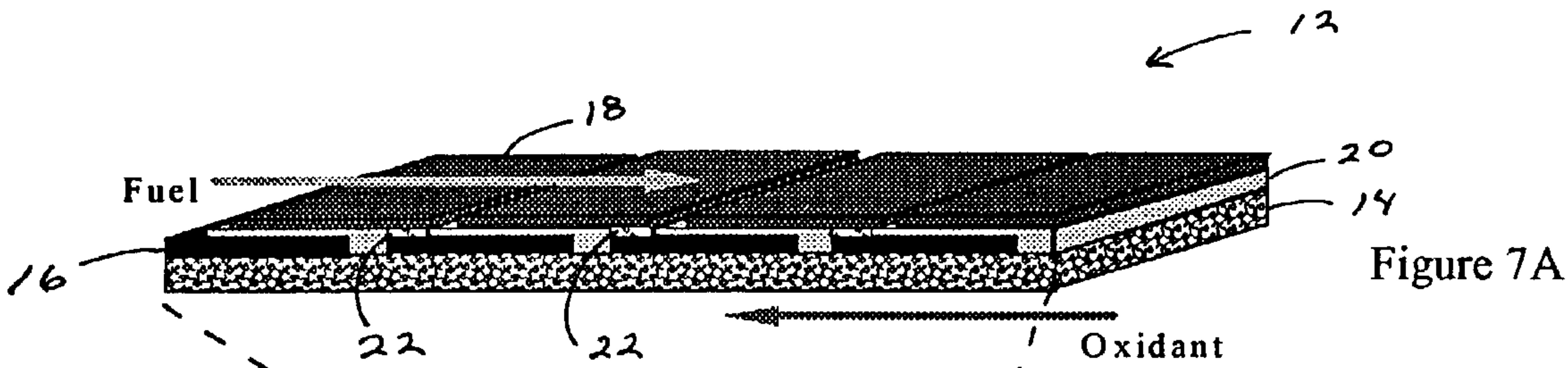
**FIGURE 3**

**FIGURE 4**

Fuel	Anode	500°C	550°C	600°C
wet ethane	Ni(10)-YDC	carbon-free conditions		carbon deposition conditions
	Ni(20)-YDC			
	Ni(40)-YDC			
dry ethane	Ni(10)-YDC			
	Ni(40)-YDC			

FIGURE 5

**FIGURE 6**



- Compare 10cm x 10cm SOFC and ISOFC
- Assumptions: 0.5 W/cm^2 at 0.7V , $0.2 \Omega \text{ cm}^2$ contact resistance

	SOFC	ISOFC
Number of Cells	1	45
Single cell area	100 cm^2	2 cm^2
Voltage	0.7V	31.5V
Current	70A	1.4A
Voltage Loss	0.14V (20%)	0.14V (0.5%)

FIGURE 8

$$R_{\Omega} = \rho L^2 / 2t_e$$

ρ = electrode resistivity (LSM $\approx 7 \times 10^{-3} \Omega\text{cm}$; Ni-YSZ $\approx 2 \times 10^{-3} \Omega\text{cm}$)

L = current path (cell width)

target: $R_{\Omega} = 0.05 \Omega\text{-cm}^2$

Calculated electrode thickness t_e (μm):

Cell Width	Ni-YSZ	LSM
0.5 mm	0.5	1.7
1 mm	2	7
2 mm	8	25
4 mm	32	100

FIGURE 9

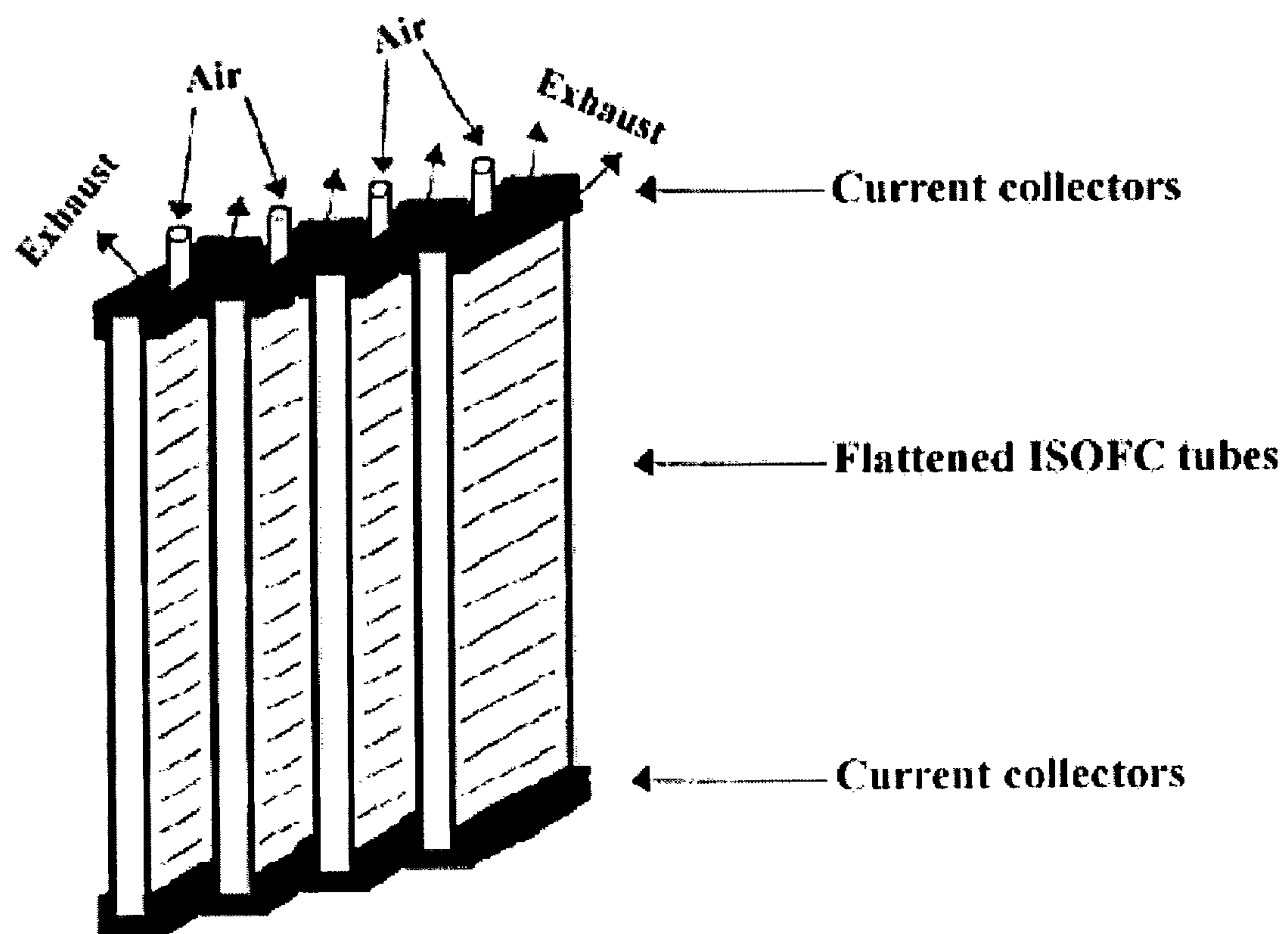


FIGURE 10

	Low T	Very Low T
Electrolyte	YSZ	Doped Ceria
Cathode	LSM	LSCF
Anode	Ni-YSZ	Ni-Ceria
IC	LSC	LSC
Support	PSZ	MgO

- IC is thin so low σ is okay. Replace (La,Sr)CrO₃?
- PSZ: TCE close to YSZ, relatively low ionic conductivity, and high fracture toughness.
- MgO: high thermal conductivity, TCE (13.5×10^{-6}) close to Ceria (12.5×10^{-6}).

FIGURE 11

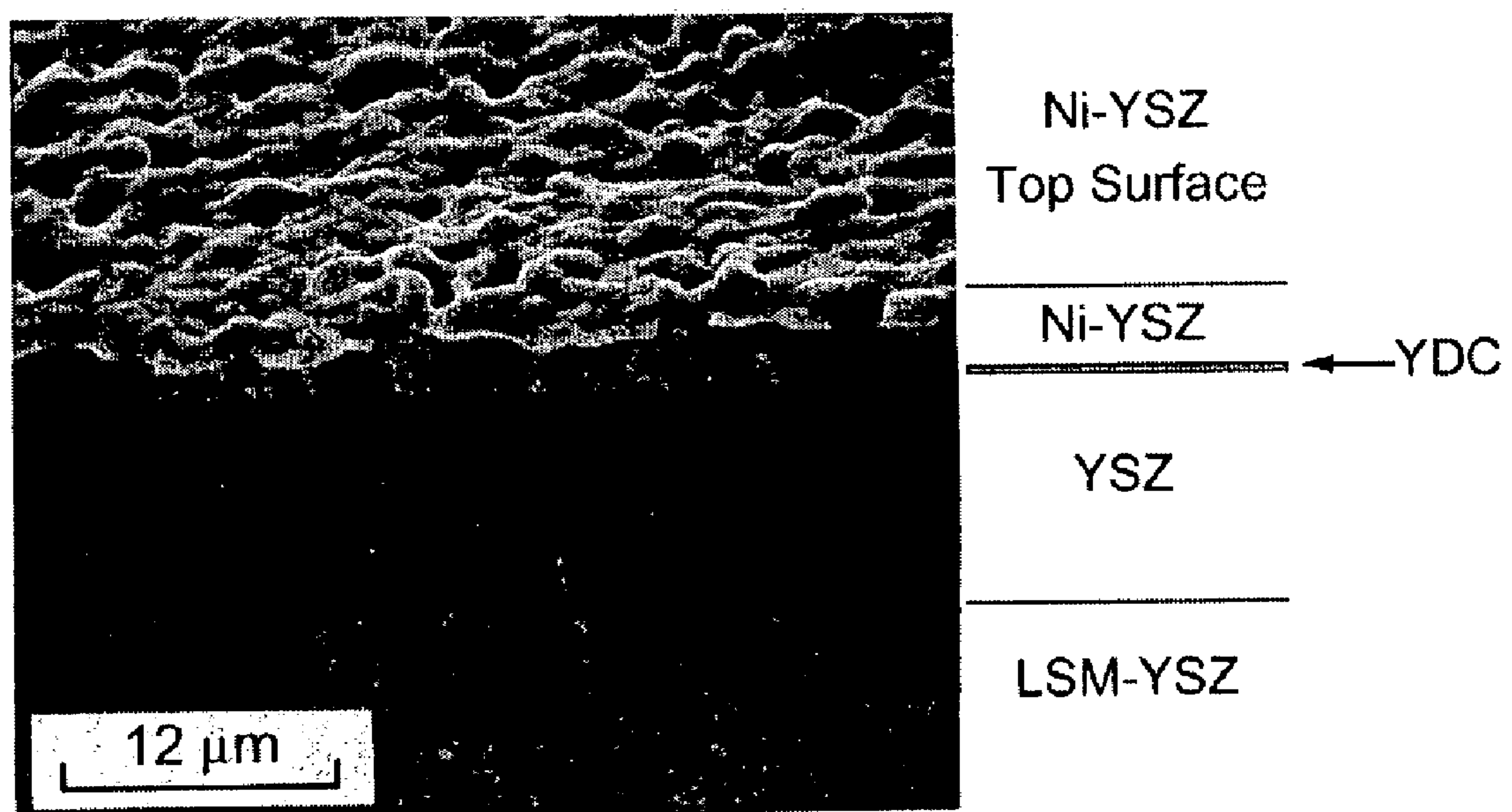
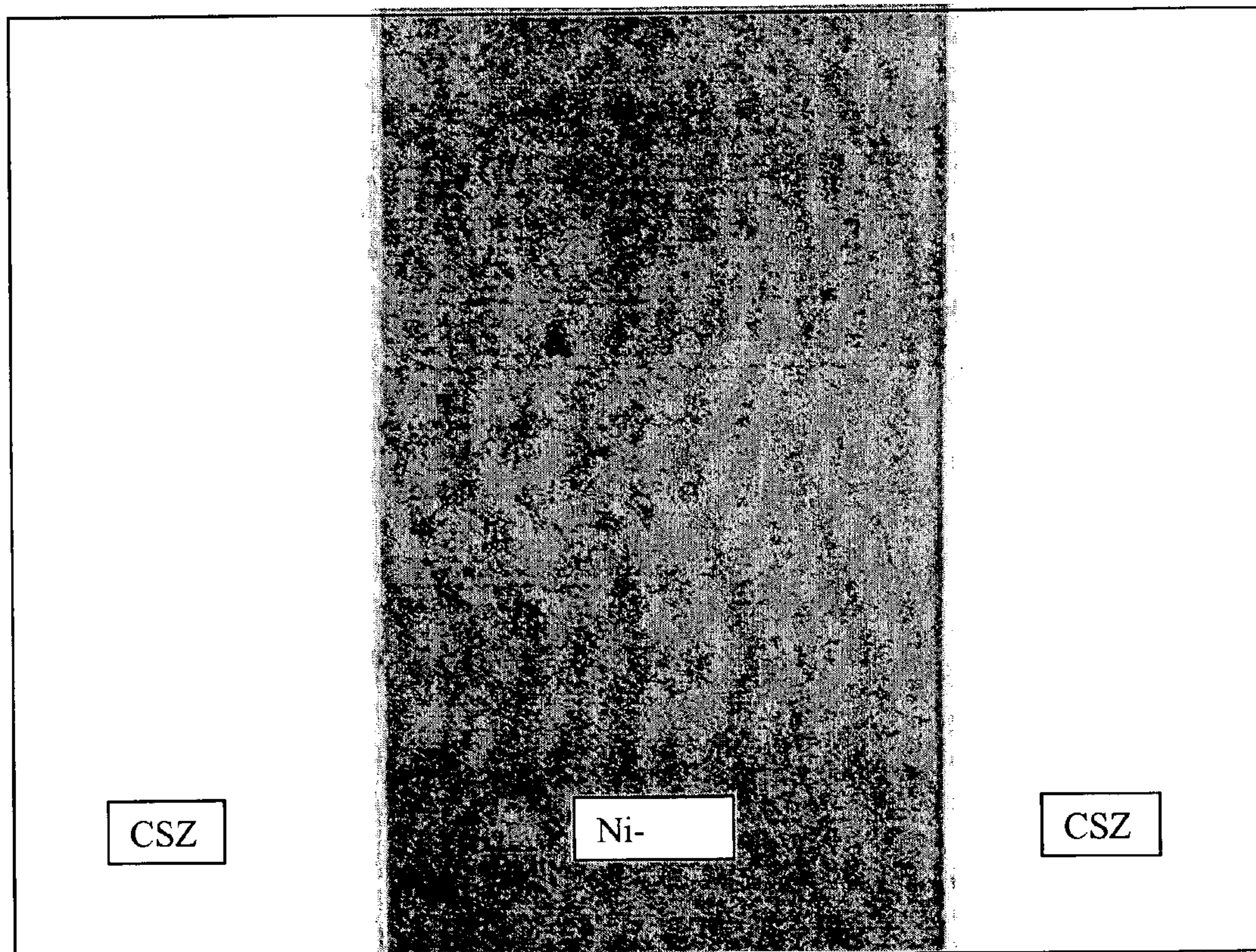


FIGURE 12



1 mm

FIGURE 13

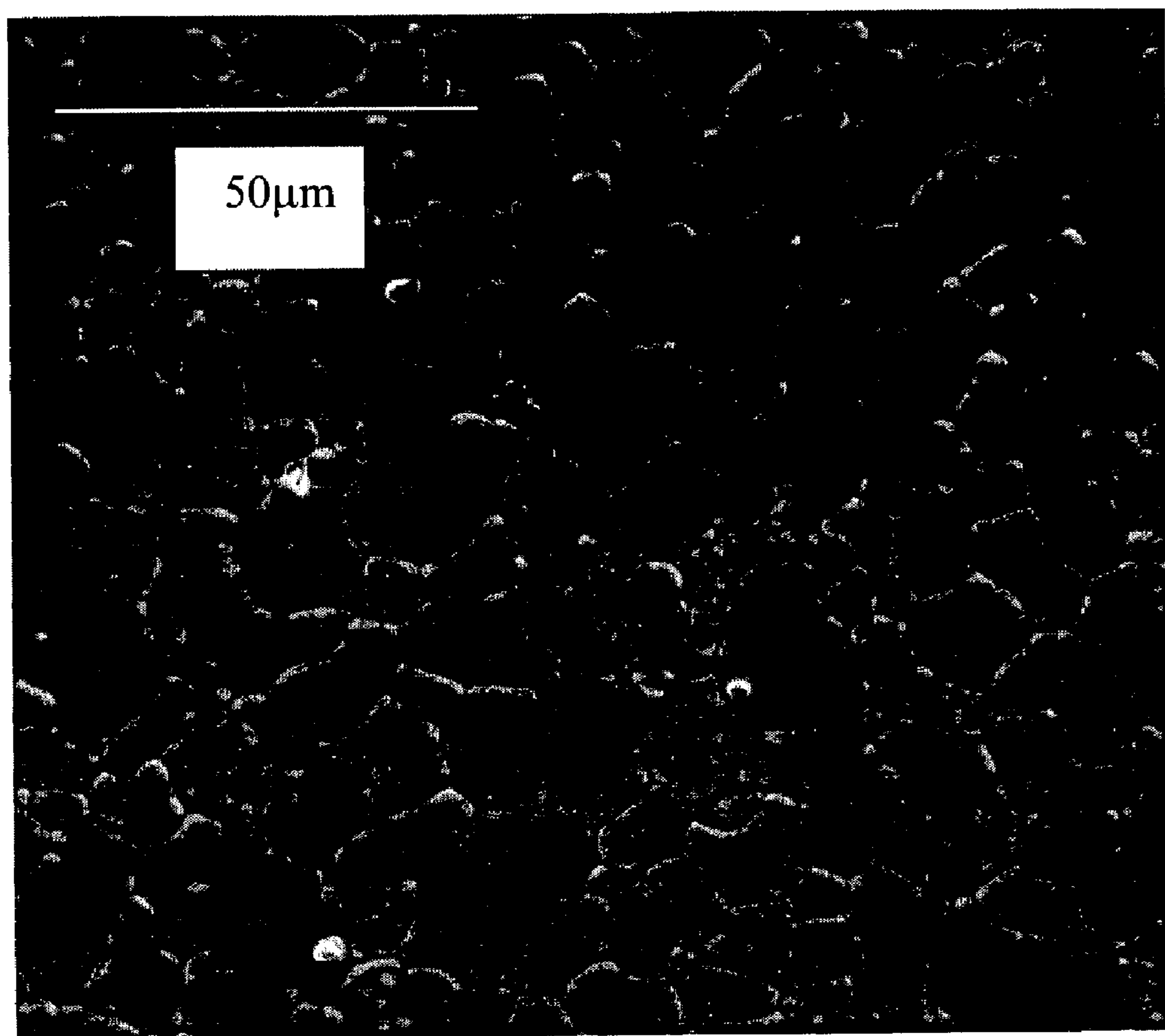


FIGURE 14

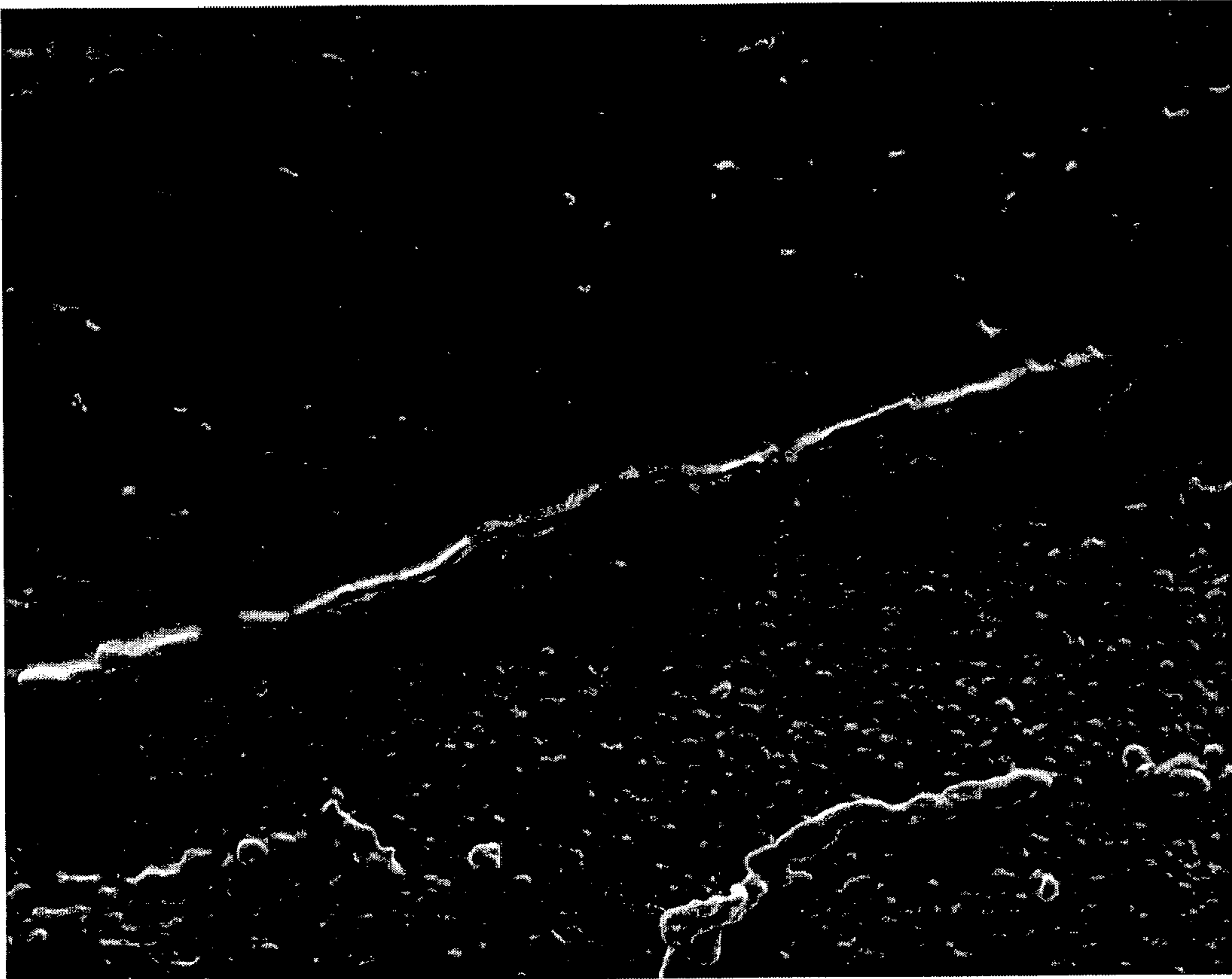


FIGURE 15

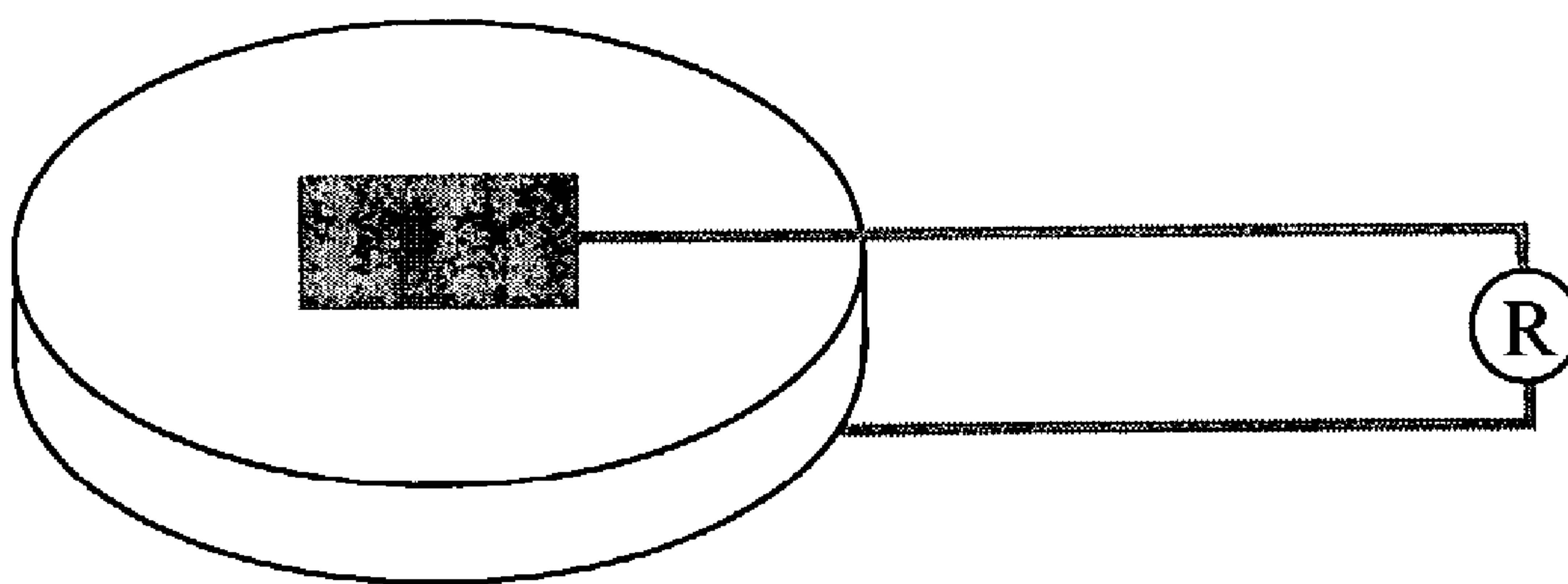


FIGURE 16

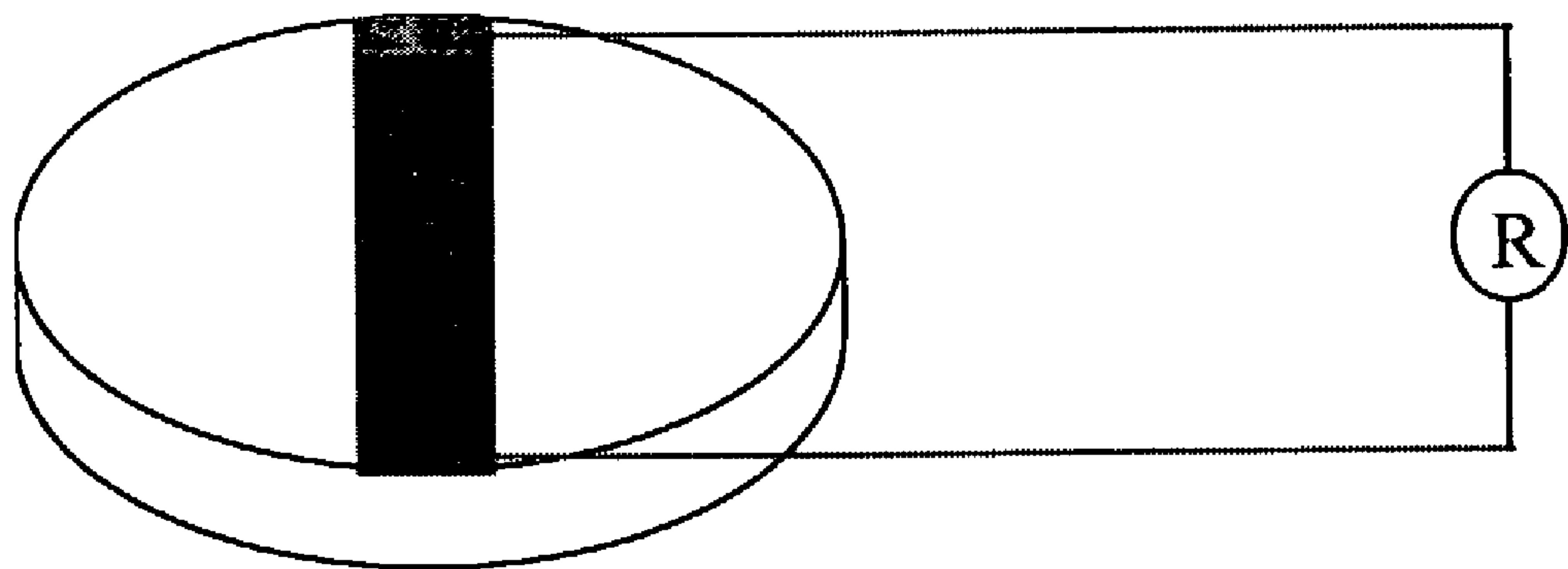


FIGURE 17

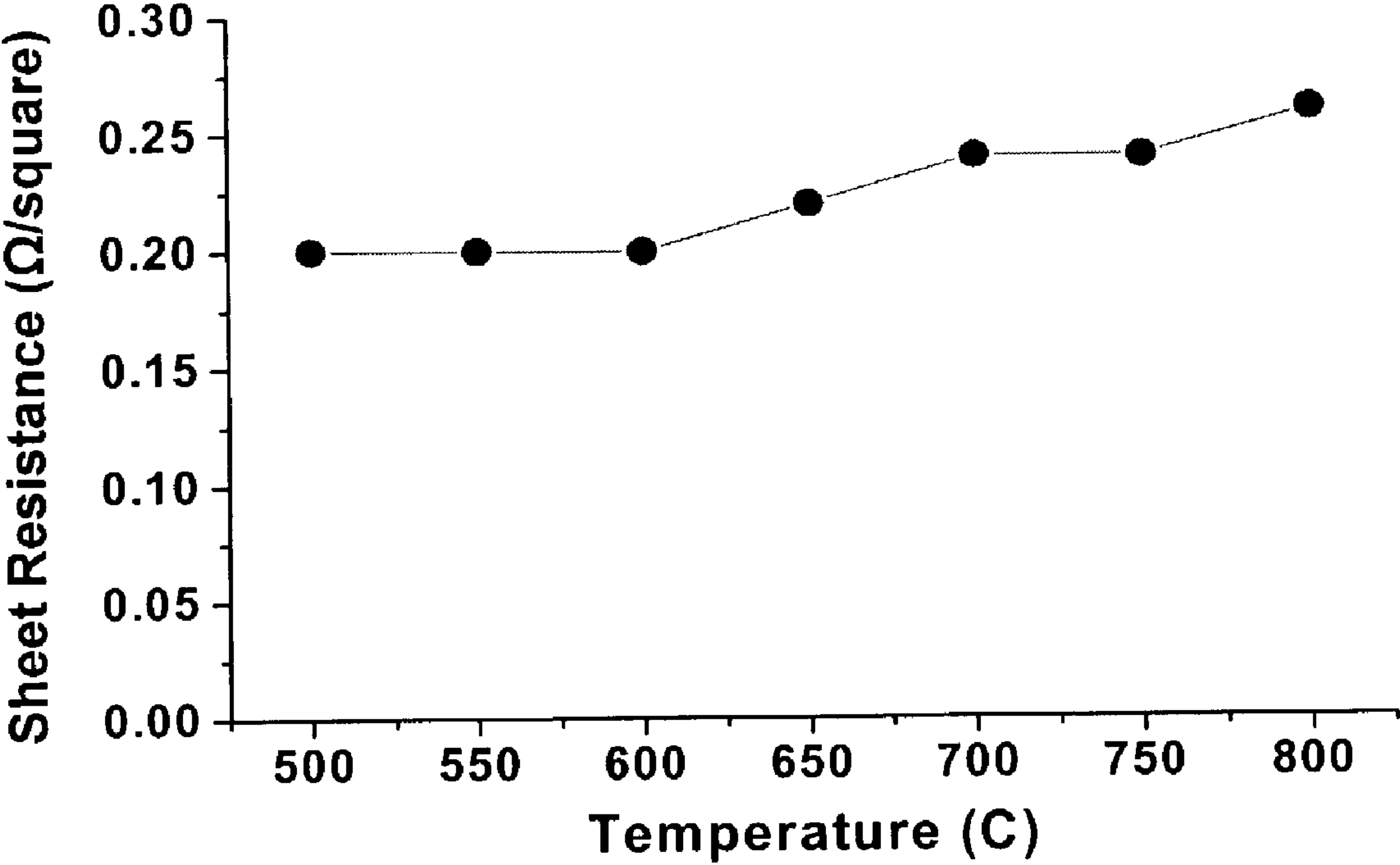


FIGURE 18

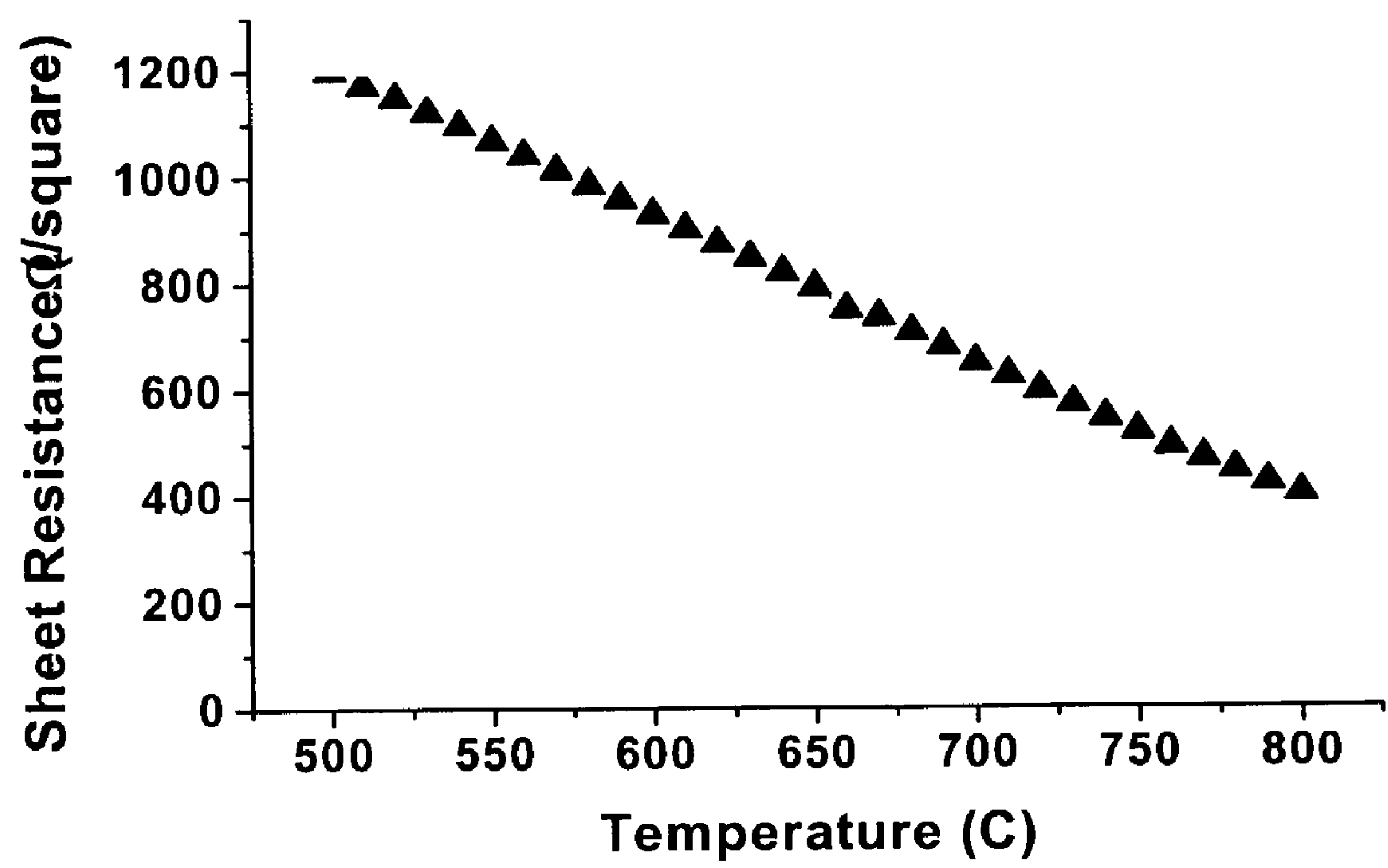


FIGURE 19

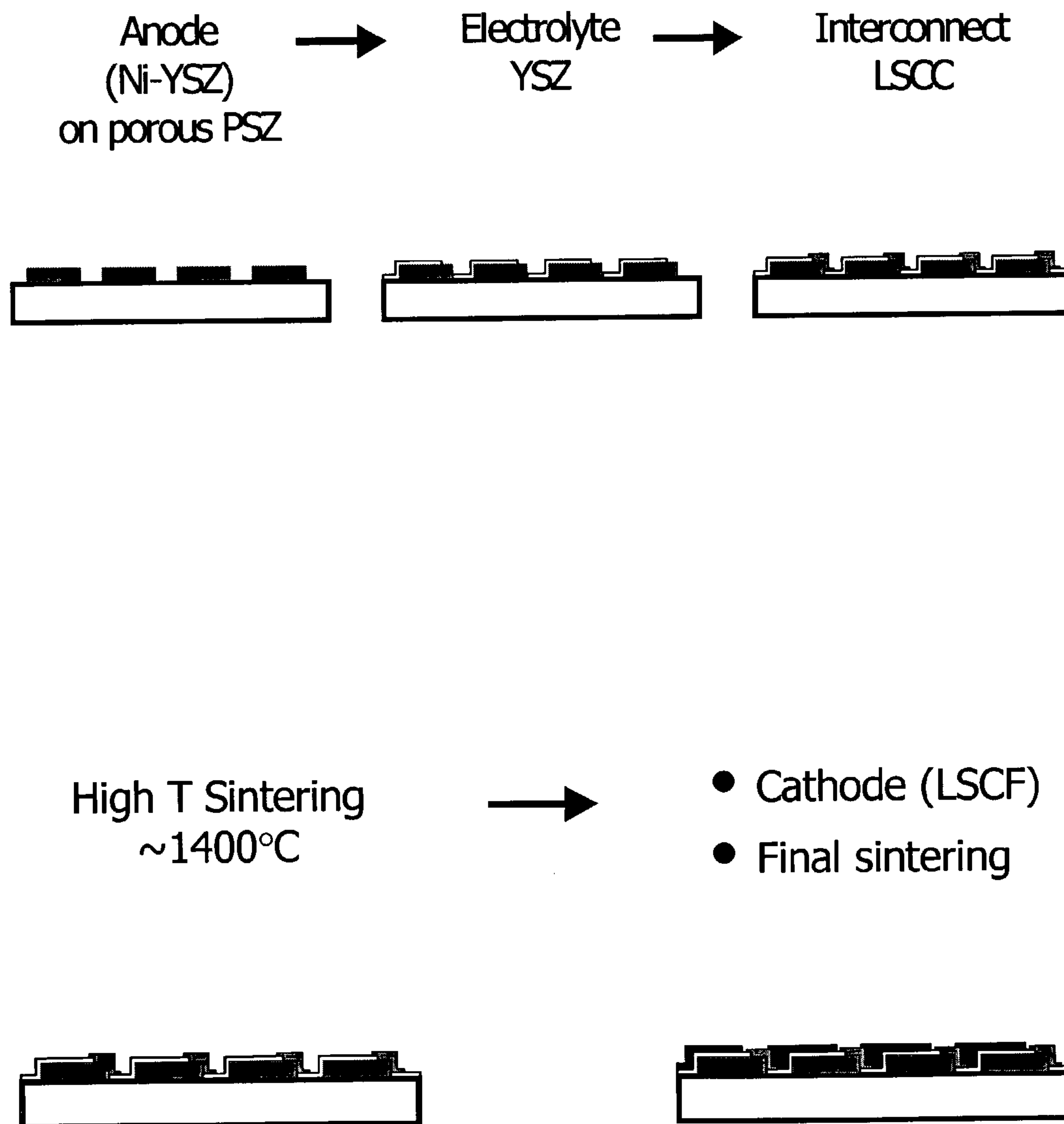


FIGURE 20

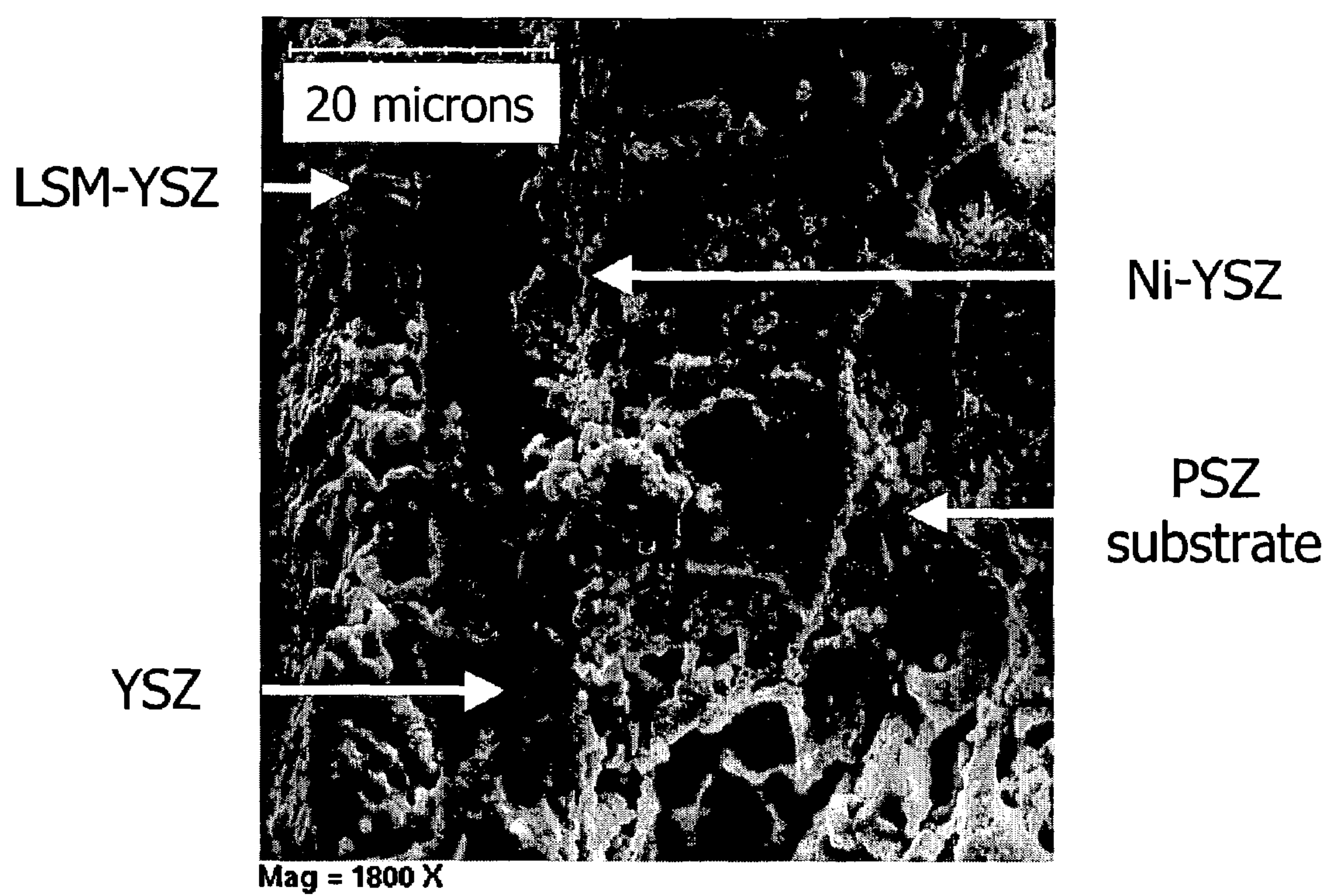


FIGURE 21

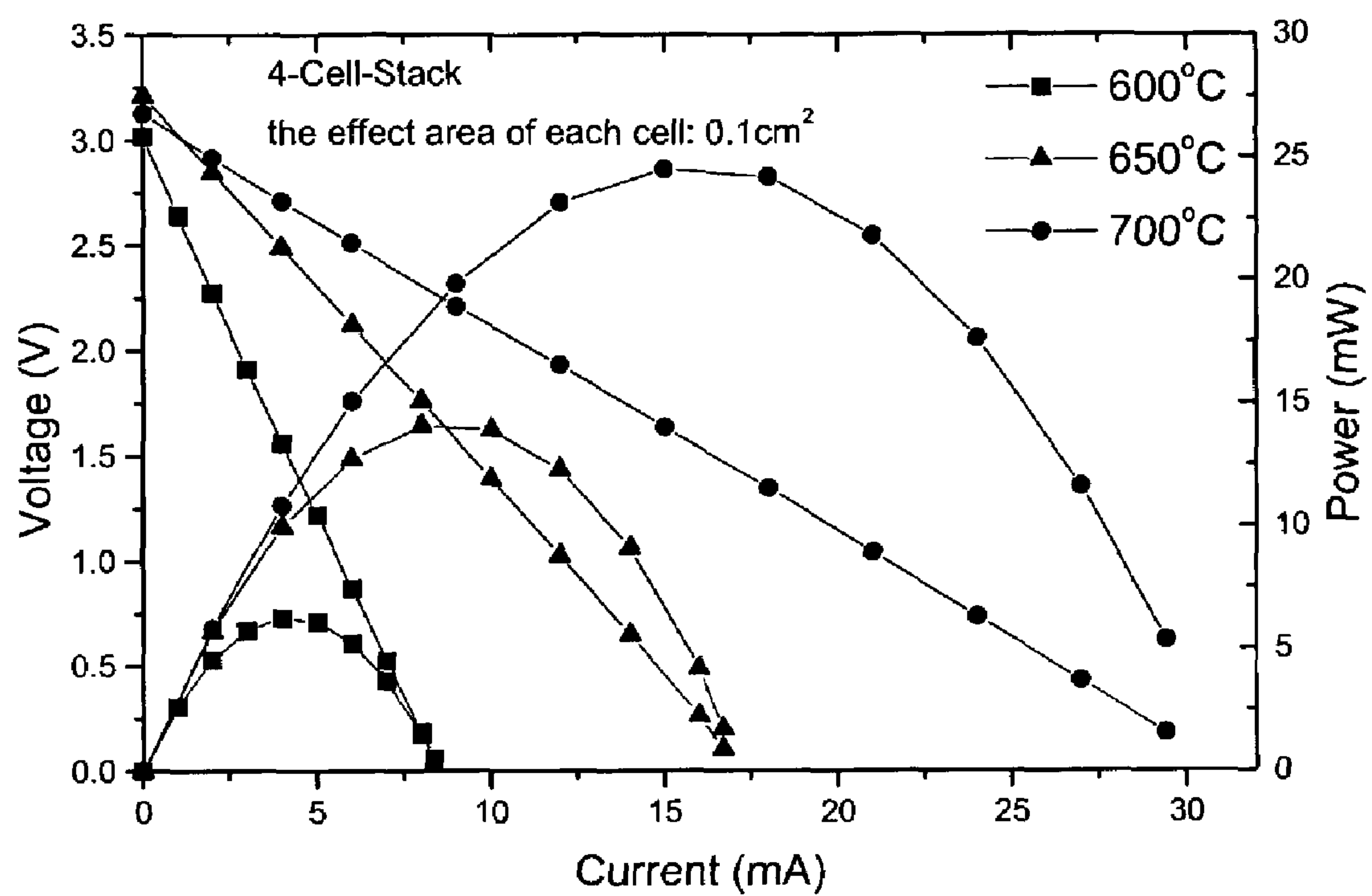


FIGURE 22

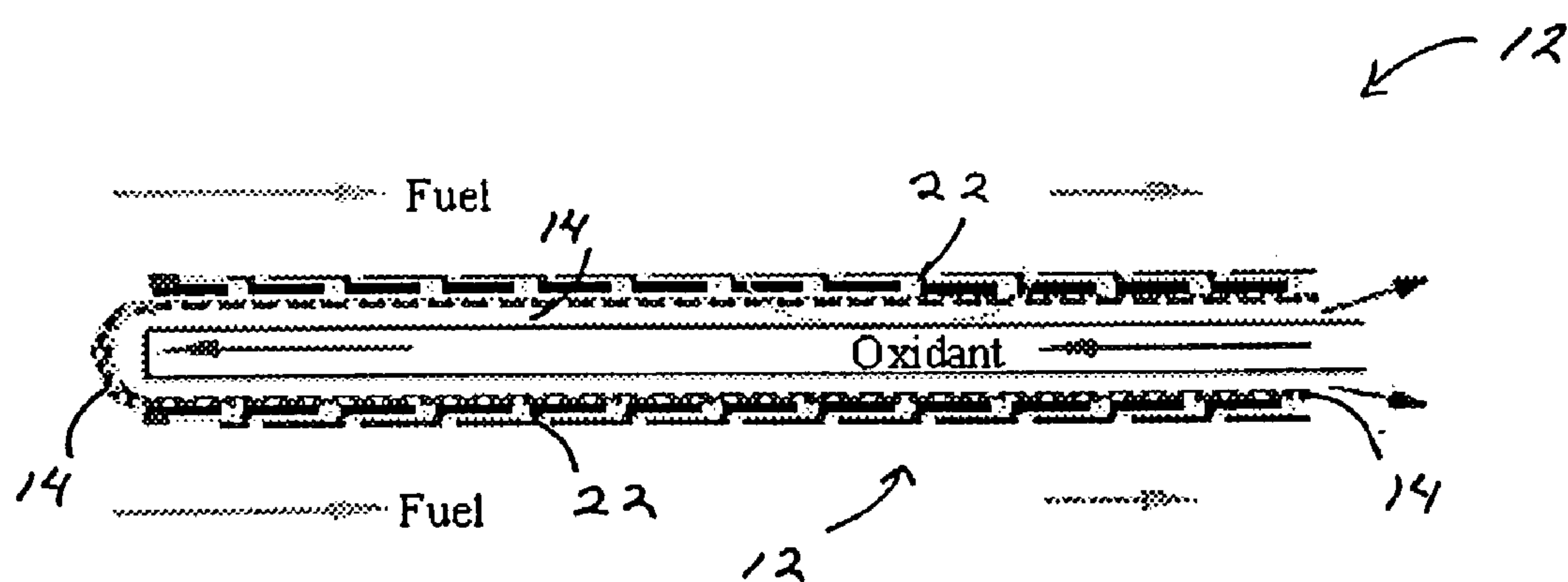


Figure 23

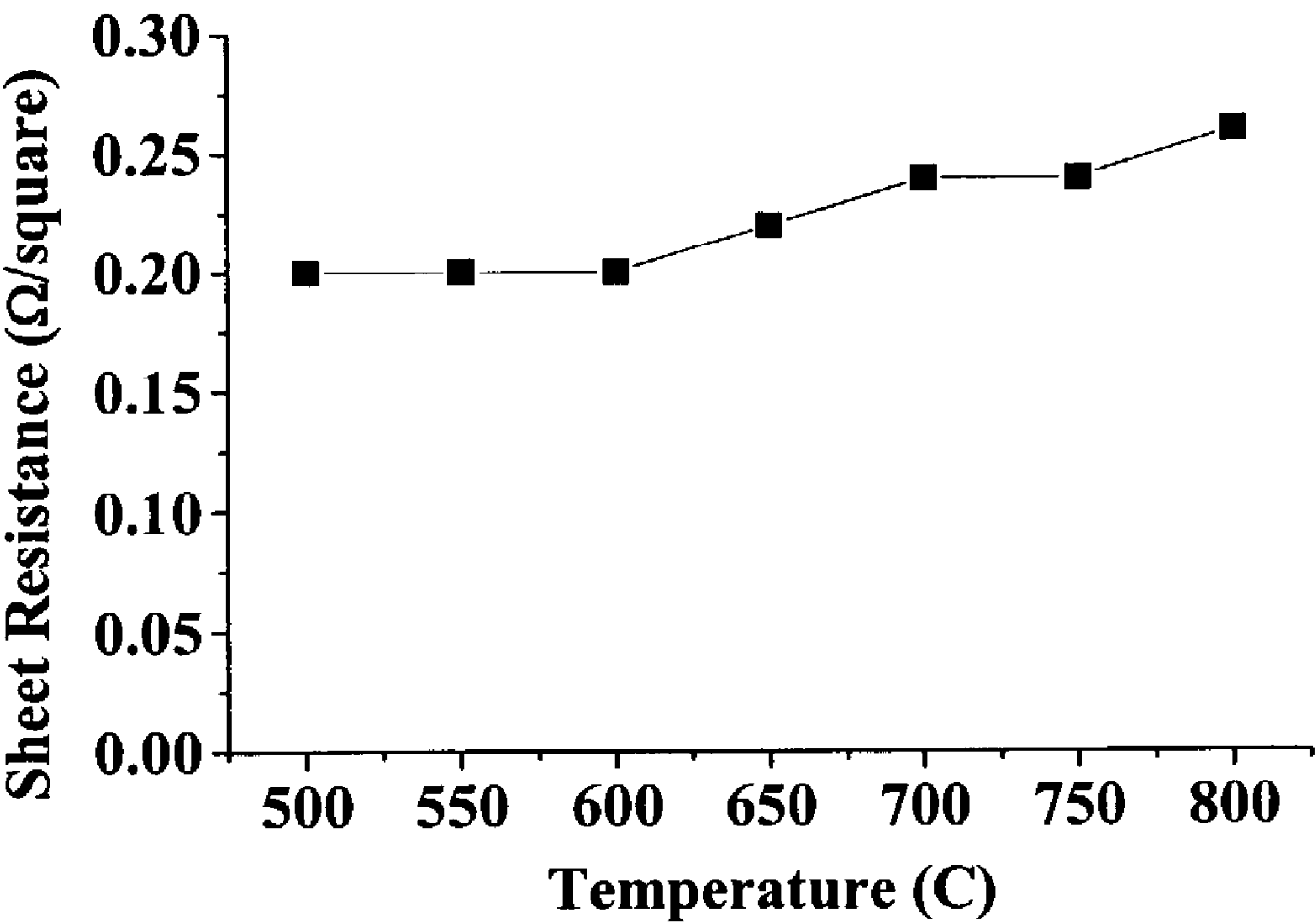
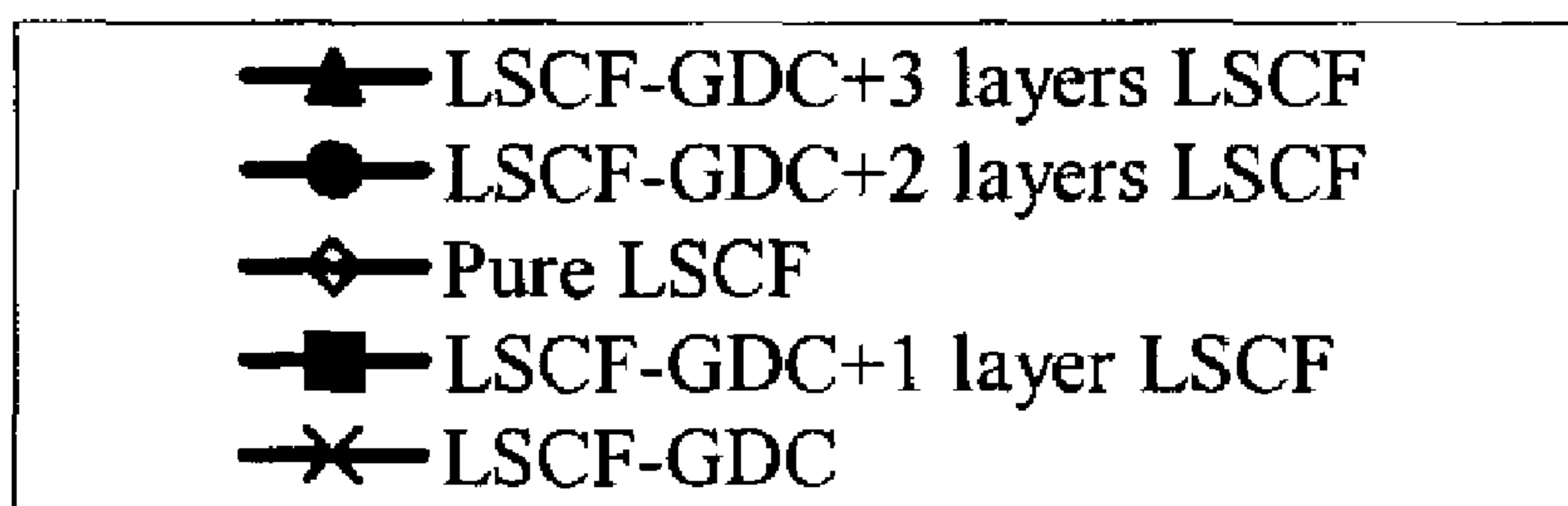
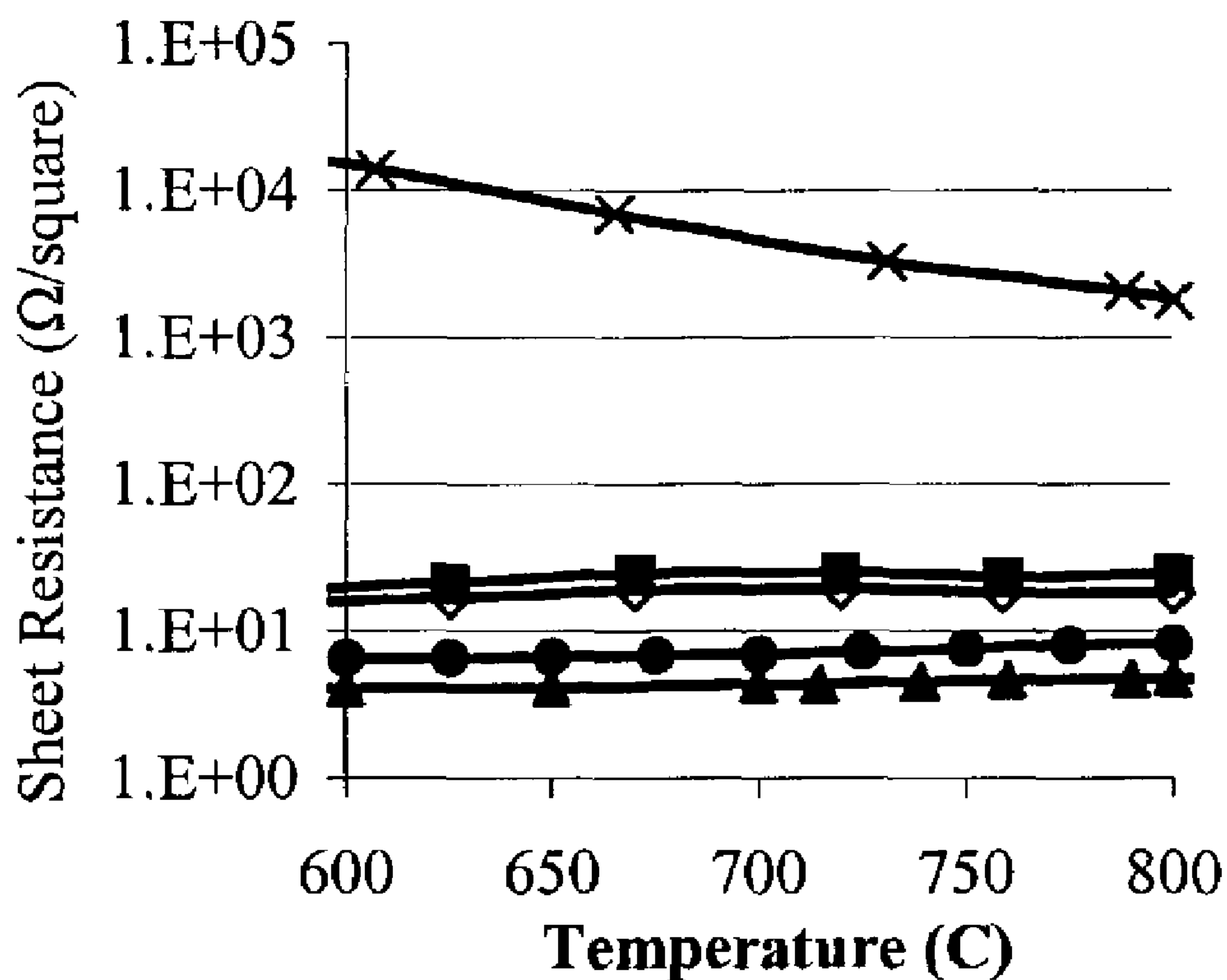
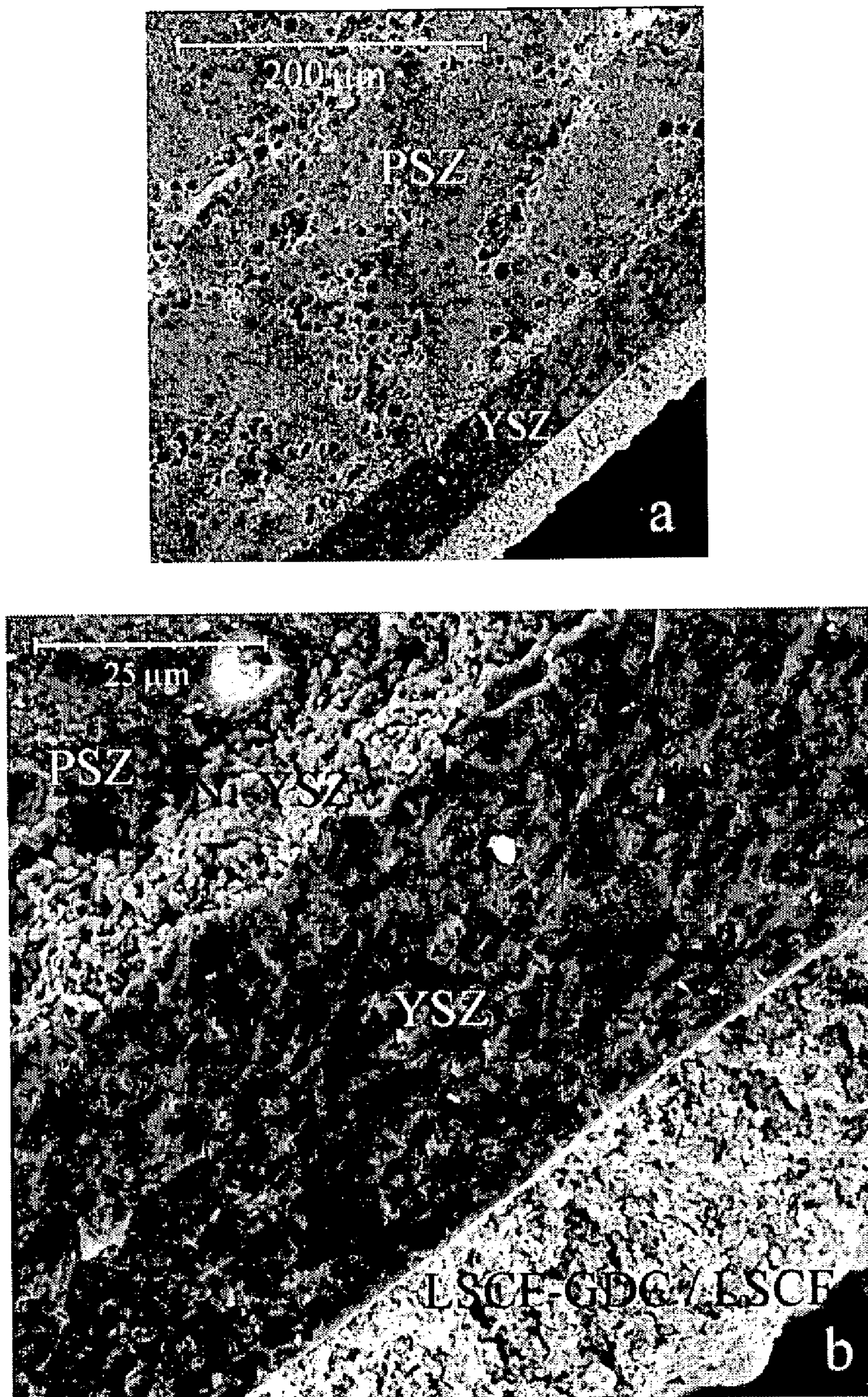
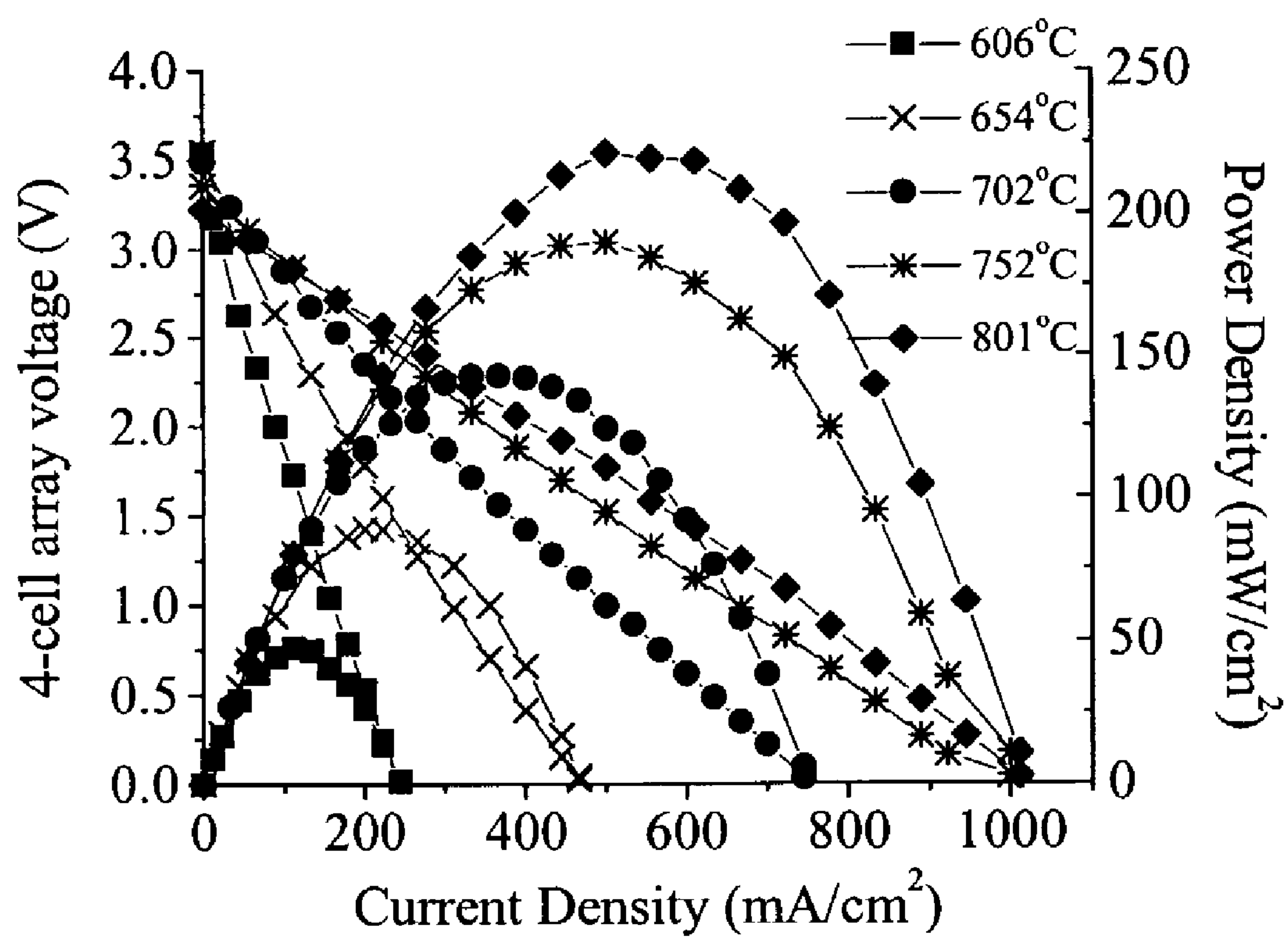


FIGURE 24

**FIGURE 25**

**FIGURE 26**

**FIGURE 27**

DIRECT HYDROCARBON FUEL CELLS

This is a continuation-in-part application of and claims priority benefit from pending International Application PCT/US02/11050, with an international filing date of Apr. 9, 2002, published in English under PCT Article 21(2), designating the United States of America, and U.S. application Ser. No. 09/833,209, filed on Apr. 10, 2001, now issued as U.S. Pat. No. 6,479,178, each of which is incorporated herein in its entirety.

The United States government has certain rights to this invention pursuant to Grant No. DE-G626-00NT40814 from the Department of Energy to Northwestern University.

FIELD OF THE INVENTION

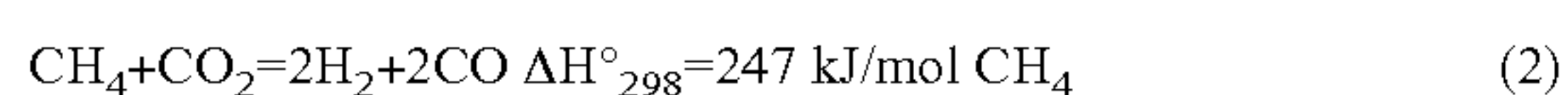
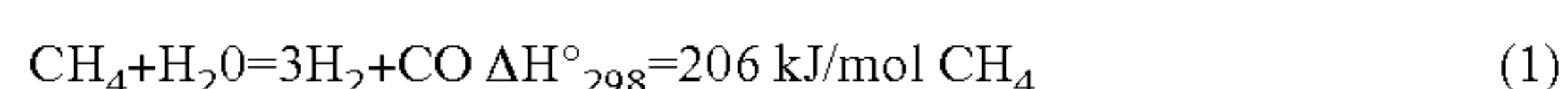
This invention relates generally to fuel cells and assemblies, more particularly, cells and components thereof as can be configured for use with hydrogen fuel or the direct oxidation of hydrocarbons.

BACKGROUND OF INVENTION

Fuel cells are promising electrical power generation technologies, with key advantages including high efficiency and low pollution. Most potential near-term applications of fuel cells require the use of hydrocarbon fuels such as methane, for which a supply infrastructure is currently available. However, fuel cells typically operate only with hydrogen as the fuel. Thus, current demonstration power plants and planned fuel-cell electric vehicles must include a hydrocarbon fuel reformer to convert the hydrocarbon fuel to hydrogen. Fuel cells that could operate directly on hydrocarbon fuels would eliminate the need for a fuel reformer, providing considerable system and economic advantages and presumably improving the viability of the technology.

Prior art fuel cells utilizing hydrocarbon fuels directly have encountered significant problems. For example, direct-methanol polymer electrolyte fuel cells produce relatively low power densities and require prohibitively large Pt loading of the anodes. In addition, methanol can permeate the electrolyte. See, for instance, Ren, X., Wilson, M. S. and Gottesfeld, S. High performance direct methanol polymer electrolyte fuel cells. *J. Electrochem. Soc.*, 143, L12-L14 (1996); and Wang, J., Wasmus, S. and Savinell, R. F. Evaluation of ethanol, 1-propanol, and 2-propanol in a direct oxidation polymer-electrolyte fuel cell a real-time mass spectrometry study. *J. Electrochem. Soc.*, 142, 4218-4224 (1995). Furthermore, only alcohol fuels appear feasible with this approach.

Alternatively, prior art solid oxide fuel cells (SOFCs) can utilize hydrocarbons directly via internal or external reforming. In this approach, a hydrocarbon fuel (e.g., methane) is combined with H₂O and/or CO₂, which are typically obtained by recirculating the fuel cell exhaust, and introduced directly to the SOFC anode. Commonly used Ni-based anodes provide the catalyst for the endothermic reforming reactions,



However, maintaining appropriate gas composition and temperature gradients across a large area SOFC stack is challenging. See, Janssen, G. J. M., DeJong, J. P., and Huijsmans, J. P. Internal reforming in state-of-the-art SOFCs. 2nd European Solid Oxide Fuel Cell Forum, 163-172, Ed. by Thorstense, B. (Oslo/Norway, 1996); and Hendriksen, P. V., Model study of internal steam reforming in SOFC stacks.

Proc. 5th Int. Symp. on Solid Oxide Fuel Cells, 1319-1325, Ed. by U. Stimming, S. C. Singhal, H. Tagawa, and W. Lehner (Electrochem. Soc., Pennington, 1997).

For instance, if the reforming reactions are slow, then insufficient H₂ is supplied to the SOFCs. On the other hand, fast reforming reactions cause cooling localized near the fuel inlet, leading to poor cell performance, and possible cell fracture. Thus, current SOFC stacks of the prior art do not take full advantage of internal reforming; rather, they employ a combination of $\approx 75\%$ external and 25% internal reforming of hydrocarbon fuels. See, Ray, E. R. Westinghouse Tubular SOFC Technology, 1992 Fuel Cell Seminar, 415-418 (1992).

SOFCs can in principle operate by direct electrochemical oxidation of a hydrocarbon fuel. This approach would be desirable since it eliminates the problems with internal reforming mentioned above, and the theoretical maximum fuel efficiency is as good or better than that for reforming. However, prior art attempts with SOFCs operating at temperatures $T_c = 900\text{-}1000^\circ \text{C}$. with methane fuel have been less than satisfactory: either power densities were very low or carbon deposition was observed. See, Putna, E. S., Stubenrauch, J., Vohs, J. M. and Gorte, R. J. Ceria-based anodes for the direct oxidation of methane in solid oxide fuel cells, *Langmuir* 11, 4832-4837 (1995); and Aida, T., Abudala, A., Ihara, M., Komiyama, H. and Yamada, K. Direct oxidation of methane on anode of solid oxide fuel cell. Proc. 4th Int. Symp. on Solid Oxide Fuel Cells, 801-809, Ed. by Dokiya, M., Yamamoto, O., Tagawa, H. and Singhal, S. C. (Electrochem. Soc. Pennington, 1995).

Recently, SOFCs have been developed to produce high power densities with hydrogen at reduced temperatures, $T_c = 600\text{-}800^\circ \text{C}$. See, Huebner, W., Anderson, H. U., Reed, D. M., Sehlin, S. R. and Deng, X. Microstructure property relationships of NiZrO₂ anodes. Proc. 4th Int. Symp. on Solid Oxide Fuel Cells, 696-705, Ed. by Dokiya, M., Yamamoto, O., Tagawa, H. and Singhal, S. C. (Electrochem. Soc. Pennington, 1995); daSouza, S., Visco, S. J. and DeJonghe, L. C. Thin-film solid oxide fuel cell with high performance at low-temperature. *Solid State Ionics* 98, 57-61 (1997); Fung, K.-Z., Chen, J., Tanner, C. and Virkar, A. V. Low temperature solid oxide fuel cells with dip-coated YSZ electrolytes. Proc. 4th Int. Symp. on Solid Oxide Fuel Cells, 1018-1027, Ed. by Dokiya, M., Yamamoto, O., Tagawa, H. and Singhal, S. C. (Electrochem. Soc. Pennington, 1995); Minh, N. Q. Development of thin-film solid oxide fuel cells for power generation applications. Proc. 4th Int. Symp. on Solid Oxide Fuel Cells, 138-145, Ed. by Dokiya, M., Yamamoto, O., Tagawa, H. and Singhal, S. C. (Electrochem. Soc. Pennington, 1995); Godickemeier, M., Sasaki, K. and Gauckler, L. J. Current-voltage characteristics of fuel cells with ceria-based electrolytes. Proc. 4th Int. Symp. on Solid Oxide Fuel Cells, 1072-1081, Ed. by Dokiya, M., Yamamoto, O., Tagawa, H. and Singhal, S. C. (Electrochem. Soc. Pennington, 1995); Tsai, T. and Barnett, S. A. Increased solid-oxide fuel cell power density using interfacial ceria layers. *Solid State Ionics* 98, 191-196 (1997); and Tsai, T., Perry, E. and Barnett, S. Low-temperature solid-oxide fuel cells utilizing thin bilayer electrolytes. *J. Electrochem. Soc.*, 144, L130-L132 (1997). However, such systems have not been considered or used for direct-hydrocarbon operation, because carbon deposition reaction rates decrease with decreasing temperature. In fact, there are no known reports SOFC operation on hydrocarbons at $T_c < 800^\circ \text{C}$.

SOFCs and related stacking configurations have undergone considerable development over the past decade. Tubular-cell-based technologies appear to be a promising approach for SOFC stacking. Tubular stacks avoid sealing

and manifolding problems inherent to planar stacks, but take a large volume for a given cell active area and can show significant ohmic losses related to current transport around the tube circumference through the (La,Sr)MnO₃ (LSM) cathode. Another problem is the relatively poor mechanical toughness of LSM. [N. M. Sammes, R. Ratnaraj, and C. E. Hatchwell, *Proceedings of the 4th International Symposium on Solid Oxide Fuel Cells*, Ed. By Dokiya, O. Yamamota, H. Tagawa, and S. C. Singhal (Electrochemical Society, Pennington, 1995) p. 952. B. Krogh, M. Brustad, M. Dahle, J. L. Eilertsen, and R. Odegard, *Proceedings of the 5th International Symposium on Solid Oxide Fuel Cells*, Ed. By U. Stimming, S. C. Singhal, H. Tagawa, and W. Lehnert (Electrochemical Society, Pennington, 1997) p. 1234.] This is typical of SOFC ceramic materials, which are optimized for electrical properties rather than mechanical toughness.

Alternatively, planar stacks can provide higher power-to-volume ratios than tubular stacks, but are not as mechanically robust as tubes and require excellent seals. Another problem with many planar stack designs is that they require pressure contacts between separate SOFC and interconnect plates. This places stringent requirements on the flatness of large-area ceramic plates, making manufacturing difficult and expensive. Furthermore, there are often relatively high resistances associated with these contacts, which deleteriously affect stack performance. It is clear that a choice between tubular and planar stacks involves trade-offs. Even so, the disadvantages associated with each respective approach present obstacles for effective use of SOFCs and suggest a new direction is needed to better utilize and benefit from this technology.

OBJECTS OF THE INVENTION

There are a considerable number of problems and the deficiencies associated with the use of hydrocarbons with solid oxide fuel cells. There is a demonstrated need for the use of such fuels in an efficient, economical fashion so as to improve the viability of the related technology.

Accordingly, it is an object of the present invention to provide various solid oxide fuel cells and/or components which can be used with hydrocarbon fuels thereby overcoming various deficiencies and shortcomings of the prior art, including those outlined above. It will be understood by those skilled in the art that one or more aspects of this invention can meet certain objectives, while one or more other aspects can meet certain other objectives. Each objective may not apply equally, in all instances, to every aspect of the present invention. As such, the following objects can be used in the alternative with respect to any one aspect of the present invention.

It can be an object of the present invention to increase the rate of hydrocarbon oxidation so as to increase and/or otherwise provide useful power densities. Such densities can be increased and/or provided utilizing various catalytic metals in the fabrication of fuel cell anodes, such anodes as can be used in conjunction with a ceria material.

It can be an object of the present invention to utilize solid oxide fuel cells and/or components thereof for low temperature direct hydrocarbon oxidation.

It can also be an object of the present invention to provide various anodes and related cellular components having small particle size obtainable by sputter deposition processes and/or related fabrication techniques.

It can also be an object of the present invention to provide a method for hydrocarbon oxidation, at a temperature lower than 800° C. and/or at a temperature for a specific hydrocarbon whereby there is no carbon deposition.

It can also be an object of the present invention to improve the viability of solid oxide fuel cells, both those described herein as well as those otherwise known in the art, through use of a unique assembly of such cells having a configuration and/or geometry of the type described herein. In particular, it is an object of this invention to provide a cell geometry/configuration whereby all active fuel cell components and interconnects are deposited as thin layers on an electrically insulating support.

It can also be an object of the present invention, in conjunction with one or more of the preceding objectives, to provide a geometry/configuration for an assembly of solid oxide fuel cells whereby assembly design and choice of support material can enhance mechanical durability and thermal shock resistance. A related objective is to decrease overall material cost by providing all cell-active materials in thin layer/film form.

It can also be an object of the present invention to improve a number of solid oxide fuel cell performance or function parameters through integration of the cell components and interconnects on a common support, such advantages including reduction of electrical resistances and interconnect conductivity requirements. As described more fully below, such integration can be accomplished through use of the thin film/layer configurations and related geometries described herein.

Another object of this invention is to provide a cell assembly configuration suitable for SOFCs of the type described herein, especially those operable at low temperatures for direct oxidation of hydrocarbon fuels, such cells as can be prepared to preferentially incorporate the catalytic metal anodes of this invention.

Other objects, features, benefits and advantages of the present invention will be apparent from the following summary and descriptions, and will be readily apparent to those skilled in the art made aware of this invention and having knowledge of various and solid oxide fuel cells in the use of hydrocarbon fuels. Such objects, features, benefits and advantages will be apparent from the above as taken in conjunction with the accompanied examples, tables, data and all reasonable inferences to be drawn therefrom.

SUMMARY OF THE INVENTION

The present invention provides for the low-temperature operation of SOFCs using hydrocarbon fuels. High power densities were obtained via direct electrochemical oxidation, without carbon deposition. The results shown herein can be extendable to fuel cell stack operation. In particular and without limitation, the present invention demonstrates the feasibility of direct hydrocarbon electrochemical oxidation in novel low-temperature solid oxide fuel cells. For instance, power densities up to 0.37 W/cm² were measured for single cells that were operated at 650° C. with atmospheric-pressure air as the oxidant and pure methane as the fuel. The measured power densities are competitive with fuel cells operated on hydrogen. As discussed more fully below, such results can be obtained at low operating temperatures ($T_c < 800^\circ \text{C.}$) and/or by incorporating ceria in the anodes of such cells.

In part, the present invention is a method of using a solid oxide fuel cell for direct hydrocarbon oxidation. The method includes (1) providing a catalytic metal anode and a ceria material contacting the anode and (2) introducing a hydrocarbon fuel to said cell, said fuel absent carbon dioxide and/or water in an amount sufficient to convert the hydrocarbon fuel to hydrogen under cell operating conditions. As such, the method is absent a hydrocarbon reforming stage.

5

The anode of the solid oxide fuel cell can be constructed using a metal catalytic for the cracking of hydrocarbons. Such a metal includes but is not limited to Pt, Ru, Pd, Fe, Co and Ni present at weight percentages of the type described elsewhere herein. Various embodiments of the present invention can also include a lanthanum chromite. Various other preferred embodiments, including oxidation of lower molecular weight hydrocarbons, utilize nickel.

In preferred embodiments of the present invention, the ceria material includes a dopant. Such dopants include but are not limited to various oxides of yttrium, gadolinium and samarium. Highly preferred embodiments include a yttria-doped ceria, having the stoichiometric relationship of $(Y_2O_3)_x(CeO_2)_{1-x}$, where "x" can be about 0.1 to about 0.25. One such embodiment is $(Y_2O_3)_{0.15}(CeO_2)_{0.85}$, although other such stoichiometries would be known, to those skilled in the art made aware of this invention, to provide a similar or comparable functional result.

With reference to use of a nickel metal and only by way of example, the catalytic anode can comprise a nickel composite. Such a composite can further include ceria and/or zirconia materials or layers of such materials used in conjunction with the nickel metal. Zirconia can be introduced to such a composite as an electrolyte adjacent to and/or contacting the anode. In preferred zirconia embodiments, various dopants can also be utilized, such dopants including but not limited to calcium, scandium, and yttrium. As would be well-known to those skilled in the art and made aware of this invention, other electrolytes can be used, including ceria, strontium-doped lanthanum gallium magnesium oxide, any of which can be doped as discussed elsewhere herein.

The method of the present invention provides for direct oxidation of hydrocarbon fuels, substantially without any reformation reaction. Fuels especially suitable for use herein include, without limitation, C_1 - C_8 alkanes, and the corresponding alcohols. Likewise, combinations of such hydrocarbons can be utilized with good effect, some mixtures for the purpose of approximating natural gas compositions.

In part, the present invention is also a method of using a ceria material to increase hydrocarbon oxidation rates in a solid oxide fuel cell. The inventive method includes (1) providing a solid oxide fuel cell having an anode composite of a catalytic metal and a ceria layer, (2) operating the cell at a temperature less than about 800°C ., (3) introducing a hydrocarbon fuel directly to the anode and (4) sorbing oxygen with the ceria layer for transfer to the anode for hydrocarbon oxidation. Solid oxide fuel cells can be constructed and/or fabricated using methods and techniques well-known to those skilled in the art, together with use of the cell components otherwise as described more fully herein. In preferred embodiments, the hydrocarbon is methane, ethane or a combination thereof, although other fuels can include those previously discussed. Irrespective of the choice of hydrocarbon fuel, preferred embodiments of such a method include operating the cell, together with its anode, at a temperature between about 500°C . and about 700°C .

In part, the present invention is also a method for suppressing and/or eliminating carbon deposition during electrochemical oxidation of a hydrocarbon in a fuel cell. The method includes (1) providing a solid oxide fuel cell anode composite of a catalytic metal and a ceria layer, (2) operating the cell at a temperature less than about 800°C ., (3) introducing the hydrocarbon directly to the anode and (4) oxidizing the hydrocarbon at the anode substantially without carbon deposition on the anode. As with other aspects of the present invention, this method can be effected using fuel cells of the prior art and/or as constructed and/or fabricated as elsewhere

6

described herein. In particular, but without limitation, the anode comprises a catalytic metal selected from the group consisting of Pt, Ru, Pd, Fe, Co and Ni. Regardless, preferred embodiments include introducing oxygen electrochemically at the anode at a rate and pressure sufficient to react the oxygen with any elemental carbon present, whereby carbon monoxide disproportionation and/or hydrocarbon pyrolysis are inhibited. While operating pressures less than 800°C . provide the desired effect, such embodiments can be employed beneficially at lower temperatures, typically between about 500°C . and about 700°C ., depending on the anode material and/or the hydrocarbon oxidized.

In part, the present invention is also an anode for direct hydrocarbon oxidation in a solid oxide fuel cell. The anode includes (1) a composite having a catalytic metal and a ceria material (2) such that the metal is present in an amount less than 60 weight percent of the anode. Catalytic metals of the present invention include those known to those skilled in the art as useful for the cracking and/or oxidation of hydrocarbons. In preferred embodiments, such a metal can include those of the type described more fully above. Regardless, the ceria material can be used with or without a dopant. In any event, the anode of this invention is substantially without carbon deposits under cell operating conditions. At lower metal levels, the present invention contemplates use of a current collector as needed to supplement conductivity.

High power density SOFCs and related methods of this invention operate by direct electrochemical hydrocarbon oxidation without carbon deposition. The anodes described herein provide for rapid hydrocarbon electrochemical oxidation rates. The results, confirmed with a simple thermodynamic analysis, show that SOFC stacks can be operated in the temperature range from ≈ 500 to 700°C - 800°C . without carbon deposition. Direct oxidation provides a desirable method for utilizing a variety of hydrocarbon fuels, avoiding the difficulties associated with reforming. Indeed, this may be the only feasible approach for low-temperature SOFCs, since extrapolation of internal reforming rate data below 750°C . suggests that reforming rates become prohibitively small.

In part, the present invention is a solid oxide fuel composite, including: (1) a substantially planar, electrically-insulating substrate; (2) a plurality of cathode components on the substrate, each cathode component spaced one from another; (3) an electrolyte on and between each cathode; (4) a plurality of anode components, each anode spaced one from another and corresponding in number to the plurality of cathode components; and (5) an interconnect component contacting the portion of each cathode component and a portion of each corresponding anode component. Such a configuration provides for fuel and oxidant cavities as shown, for instance, in FIG. 7B. Alternatively, a plurality of anode components can be deposited on a substrate, with a corresponding number of cathode components interconnected therewith. Without limitation, reference is made to FIGS. 20-21 and examples 26-27, below.

In preferred embodiments, the solid oxide fuel cell composite includes a catalytic metal anode and a ceria material contacting the anode, as described more fully above, for direct hydrocarbon oxidation. In such embodiments, the catalytic metal includes, but is not limited to, Pt, Ru, Pd, Fe, Co and Ni present at weight percentages of the type described elsewhere herein. Other embodiments, preferred or otherwise, can be utilized with comparable effect depending upon the type of fuel. Regardless, preferred embodiments of such fuel cell composites include a doped ceria material. Highly

preferred embodiments include a yttria-doped ceria having a stoichiometric relationship such as that provided elsewhere herein.

In part, the present invention can also include a solid oxide fuel cell assembly, including: (1) a substantially planar array of fuel cells on a substrate, each cell having cathode, anode, electrolyte and interconnect component structures, with each component structure of each cell having a sub-planar arrangement of one to another; (2) an oxidant cavity adjacent the substrate; and (3) a fuel cavity adjacent the sub-planar anode arrangement. As discussed above, and as further described in example 14, an assembly configured with anodes on a substrate will provide a converse cavity placement; i.e., a fuel cavity adjacent the substrate and an oxidant cavity adjacent the anodes. Fuels and oxidants useful with such cells and related assemblies are as described herein or otherwise known in the art. Likewise, the requisite cavities and supporting cellular/assembled structures will be understood upon consideration of various aspects of this invention.

As provided above and elsewhere herein, a solid oxide fuel cell assembly of this invention can also comprise (1) a substantially planar array of fuel cells upon a substrate, each cell comprising cathode, anode, electrolyte and electrode interconnect component structures, each component structure of each cell having a sub-planar arrangement of one component structure to another; and (2) a fuel cavity adjacent the sub-planar arrangement, the assembly providing reduced resistance to current flow with increased cell number. In certain embodiments of such an assembly, each fuel cell can have a width dimension of about 2 mm. In certain other embodiments, limited only by lithographic technique or fabrication method, cell dimension can be reduced down to about 0.1 mm. In conjunction therewith, either or both cathode and anode component structures can have a thickness dimension of about 10 mm.

The cell and/or component structure configuration of this invention can be used in conjunction with choice of material composition. For example, without limitation, a cathode component of such an assembly cell can comprise LSM. Regardless, an anode component can comprise Ni—YSZ. With regard to the latter, certain embodiments can be utilized in conjunction with an electrolyte comprising YSZ. As another consideration, a substrate component for such an array of cells can benefit from choice of a material having a thermal expansion coefficient matching a corresponding electrolyte parameter. With reference to a YSZ electrolyte, such a support can suitably comprise a PSZ material.

A preferred embodiment of such an assembly is illustrated in several of the following figures. In particular, a plurality of such planar arrays, configured with the corresponding oxidant and fuel cavities can provide a stacking configuration such as that portrayed in FIG. 7B.

Further consideration of the present invention, with reference to preceding examples and figures, provides a method of using reduced operating temperature to reduce current shunting loss from such a solid oxide fuel cell. An inventive method comprises (1) providing a substantially planar array of fuel cells on an ionically-conducting substrate support, each cell comprising cathode, anode, electrolyte and electrode interconnect component structures; and (2) operating the array of cells at a temperature less than about 800° C. Without limitation, certain embodiments of such a method can be effected in conjunction with a substrate support comprising a PSZ material. Regardless, reduced cell width increases voltage across the planar array. Beneficial effect is achieved with such a cell having a width dimension of about 2 mm down to about 0.1 mm. The operating temperature of such a cellular array is

between about 600° C. and about 800° C. and/or at a temperature reduced in comparison to operating temperatures of the prior art. Reference is made, more specifically but without limitation, to example 23 and the data provided therewith.

Consistent with the foregoing and various data provided herein, as supported by electrical/cell models, electrode/cathode sheet resistance can limit performance due to low measured conductivities. Smaller cell widths, dimensioned as provided in various examples and descriptions, enhance maximum power densities. As but one departure from the prior art, the pitch of an array of solid oxide fuel cells of this invention is distinguishably smaller than the value(s) reported in such prior art. The assemblies of this invention provide reduced resistance with decreased cell dimension, increased cell number and a corresponding increase in the number of interfaces per unit length of cell. Resistance loss continues to decrease as pitch decreases. As a result, with consideration of the present cell dimensions, an aspect ratio of this invention can be greater than that of the prior art but without undue concern about shunting current loss. As described herein, choice of substrate support and reduced operating temperature can serve to reduce such loss from a solid oxide fuel cell.

In part, the present invention is also a method of constructing a series of solid oxide fuel cells, such cells as can be used in conjunction with the composites and/or assemblies described above. Such a method, without limitation, includes one or more of the following constructions: (1) providing a substrate with masks aligned thereon in a predetermined pattern; (2) placing/depositing a first electrode material on the substrate; (3) re-aligning the masks on the first electrode materials, one mask on each such first electrode material; (4) placing/depositing an electrolyte material on the first electrode material; (5) removing the masks and placing/depositing an interconnect material on the first electrode material; and (6) re-aligning the masks on the electrolyte and placing/depositing a second electrode material on the electrolyte. Without limitation, for purposes of illustration, reference is made to FIG. 20 and examples 26-27, below.

Such electrode/electrolyte and/or interconnect components can be prepared and integrated on a substrate and with one another as described herein, using thin-film/layer techniques of the prior art, such techniques and straight-forward modifications thereof as would be understood by those skilled in the art made aware of this invention. Successive masking, deposition, and unmasking procedures can be employed to deposit/print cathode, electrolyte, interconnect and anode components on a suitable insulating substrate. Such procedures or fabrication steps would also be known to those skilled in the art, modified as necessary to accommodate use of the component materials described herein or to otherwise achieve the functional and/or performance characteristics desired. Fabrication in this manner on a suitable substrate, provides a planar composite, array and/or assembly of solid oxide fuel cells wherein the cells are integrated one with another. (See, for example, FIGS. 7A and 20.) The cellular stacking geometries of this invention have, therefore, the capacity to be two- or three-dimensional. Such procedures can be viewed as analogous to various thin-film/layer techniques used in the fabrication of micro- and nano-dimension integrated devices, hence the reference to integration and integrated stacks.

Individual planar, integrated assemblies can be mounted one above another and between structural components described elsewhere herein and as necessary to provide a functional fuel cell. Such end-plates/caps, fuel feed tubes and associated non-conductive seals are of well-known material choice and construction, the design of which can be as shown

in FIG. 7B or, in accordance with this invention, as necessary to provide the desired performance property or parameter.

As discussed above, SOFCs are a very promising energy conversion technology for utilization of fossil fuels and hydrocarbons produced therefrom. The present invention introduces a novel stacking geometry devised to enhance the benefits available from this technology. The geometry involved has all active SOFC components and the interconnect deposited as thin layers on an electrically insulating support. This configuration allows the choice of a support material that provides optimal mechanical toughness and thermal shock resistance. The supports can be in the form of flattened tubes, providing relatively high strength, high packing densities, and minimizing the number of seals required. The integration of SOFCs and interconnects on the same support provides several other advantages including the reduction of electrical resistances associated with pressure contacts between the cells and interconnects, relaxation of fabrication tolerances required for pressure contacts, reduction of ohmic losses, and reduction of interconnect conductivity requirements. The materials used in the integrated stacks of this invention can be similar to or the same used with conventional SOFCs, and long-term stable operation will be achievable. Use of thin layer cell-active components helps to lower overall material costs.

Without limitation as to the scope of this invention and irrespective of the fuel (hydrogen or hydrocarbon) used, the following provides several advantages, attributes and/or aspects pertaining to one or more embodiments of the stacking configurations, planar geometries and/or assemblies described herein.

1. The support is not an electrically active part of the stack; it can be designed chosen for optimal mechanical properties.

2. There are no separate interconnect pieces, and a reduction in the number of seals is possible. The cells can be fabricated in the form of flattened tubes, such that a seal-less design similar to tubular stacks can be implemented while retaining the high power-to-volume ratios of planar stacks.

3. Because the SOFC components and interconnects are in intimate contact, electrical losses related to pressure contacts are greatly reduced, improving stack performance.

4. Because no separate interconnect pieces and fewer gas-flow channels are required, there is a reduction in stack volume and weight.

5. Large integrated stack elements can be made by increasing the number of cells: there is no need to make very large area cells.

6. Considerable flexibility is provided by way of stack design: for example, individual cell sizes can be varied slightly to account for spatial variations in gas composition and temperature.

BRIEF DESCRIPTION OF THE DRAWINGS

FIG. 1A illustrates cell voltage and power density vs. current density for an SOFC operated on air and methane; FIG. 1B provides variations in operating temperature for the cell of FIG. 1A and the respective voltage and power densities observed therewith and as shown in FIG. 1A. The measurements were collected in atmospheric pressure air, and methane fuel was supplied at $\sim 50 \text{ cm}^3 \text{ STP min}^{-1}$.

FIG. 2 shows a comparison of electrode impedance spectra for Ni—YSZ/YDC anodes measured at 600° C. in (a) 97% $\text{CH}_4 + 3\% \text{ H}_2\text{O}$, (b) 3% $\text{H}_2 + 3\% \text{ H}_2\text{O} + 94\% \text{ Ar}$, and (c) 97% $\text{H}_2 + 3\% \text{ H}_2\text{O}$.

FIG. 3 compares impedance spectroscopy results for Ni—YSZ and Ni—YSZ/YDC anodes in 97% $\text{CH}_4 + 3\% \text{ H}_2\text{O}$ at 600° C.

FIG. 4 shows CO/CO₂ ratios calculated at equilibrium with graphitic carbon ($\bullet P_{\text{CO}} + P_{\text{CO}_2}$, 0.1 atm; and $\blacksquare P_{\text{CO}} + P_{\text{CO}_2}$, 0.2 atm) based on reaction (5), in Example 7.

FIG. 5 is a table showing conditions that limit and promote carbon deposition, as compared to various Ni—YDC anodes and the parenthetical reference to Ni weight percent therein. While such percentages are shown with respect to ethane and nickel-based anodes, the same can be extended with comparable effect to other anode metals and the direct oxidation of other hydrocarbons, as would be well known to those skilled in the art and made aware of this invention.

FIG. 6 compares cell power density vs. current density for a solid oxide fuel cell operated on air and ethane.

FIG. 7A shows an enlarged schematic view of an integrated stack element showing the cell-interconnect geometry.

FIG. 7B illustrates a hydrogen (or hydrocarbon) flow cavity can be created between two such stack elements by sealing at the edges. The addition of end-caps that include fuel-feed tubes results in a fully sealed geometry.

FIG. 8 provides a comparison of various performance properties and parameters associated with a typical solid oxide fuel cell (SOFC), as described, and an integrated solid oxide fuel cell (ISOFC) of this invention.

FIG. 9 demonstrates another aspect of the present invention, low lateral resistance loss and reduction thereof with cell width, as can be illustrated with Ni—YSZ and LSM cathodes.

FIG. 10 is a schematic illustration of stacked integrated solid oxide fuel cells, in accordance with this invention, showing in particular, the structural relationship and placement of various cell assembly components such as current collectors and fuel tubes.

FIG. 11 provides and compares representative materials for the cell components of this invention.

FIG. 12 is an SEM fracture cross-sectional image of a typical thin-electrolyte SOFC showing LSM-YSZ substrate, YSZ electrolyte, and Ni—YSZ anode (the thin YDC layer is not visible).

FIG. 13 is an optical micrograph showing a portion of a patterned NiO-YSZ anode layer on a CSZ support.

FIG. 14 is an SEM micrograph of the top surface of a sintered YSZ layer.

FIG. 15 is an SEM micrograph showing the masked edge of a YSZ electrolyte on Ni—YSZ. The Ni—YSZ (lower part) can be distinguished from the YSZ layer (upper part) by its smaller grain size.

FIG. 16 shows 2-point conductivity measurement of porous PSZ substrate.

FIG. 17 provides a schematic representation of an anode conductivity test.

FIG. 18 graphically illustrates the sheet resistance of a preferred screen printed Ni—YSZ anode.

FIG. 19 graphically illustrates the sheet resistance of a screen printed LSFC-GDC cathode, in accordance with this invention.

FIG. 20 shows, in schematic sequence, in cross-sectional view, planar SOFC component layers, assembled in accordance with this invention.

FIG. 21 shows a cross-sectional SEM micrograph of the screen printed component layers of the integrated solid oxide fuel cell of FIG. 20.

FIG. 22 graphically illustrates performance of a 4-cell ISOFC stack. The area of each cell is $\approx 0.1 \text{ cm}^2$.

FIG. 23 shows, schematically in cross-sectional view, a preferred array of solid oxide fuel cells, in accordance with this invention, utilizing a closed-ended tubular PSZ support.

FIG. 24 provides sheet resistance versus temperature of a $\approx 10\text{-}\mu\text{m}$ -thick screen printed Ni—YSZ anode.

FIG. 25 provides sheet resistance versus temperature of various screen printed cathode materials and multiple layers.

FIGS. 26A-B provide cross sectional SEM micrographs of the four-cell array at low magnification (A), showing the microstructure of the PSZ substrate, and at higher magnification (B), showing microstructure of SOFC active layers.

FIG. 27 plots voltage and power density versus current density for a four-cell SOFC array tested in air and humidified hydrogen at various temperatures.

DETAILED DESCRIPTION OF PREFERRED EMBODIMENTS

One schematic perspective view of an SOFC stack, in accordance with this invention, is shown in FIGS. 7A and 7B. An array of SOFCs 12, connected in series by thin-film interconnects 22, are deposited onto a porous, insulating support 14. The layers 12 can be deposited in the order: electrode (cathode or anode), electrolyte, interconnect, and electrode (cathode or anode). The patterning is such that electrolyte 20 and interconnect 22, which are both dense layers, are continuous and form a gas-tight seal over the entire surface. With respect to FIGS. 7A and 7B, the electrodes, cathode 16 and anode 18 are porous layers separated by electrolyte 20, and connected by interconnect 22. Alternatively, and as elsewhere described more fully, anodes can be positioned on the substrate and interconnected with cathodes. (See, e.g., examples 26-27 and FIG. 20.)

By contrast, in conventional planar stacks, the current flows between separate SOFC and interconnect pieces: the stacking order is hydrogen (fuel)-SOFC-oxygen-interconnect-hydrogen (fuel)-SOFC, and so forth. The polarity of the SOFCs must be maintained in order for additive voltages. In the stacks 10 of this invention, however, the current flows across the integrated stack elements. There is no requirement that the pieces be stacked with the same polarity, such that the cells can be mounted in opposite directions as shown schematically in FIG. 7B: that is, a stacking order of fuel-SOFC-oxygen-SOFC-fuel-SOFC, etc. There are no separate interconnect pieces, and the gas-flow volume per unit generator area is reduced by a factor of ≈ 2 .

FIGS. 7A and 7B illustrate a straightforward approach in which the individual planar integrated stack pieces 12 are mounted between end plates 24 and feed tubes 26, requiring seals between the stack pieces and end plates. An alternative approach is the deposit of cells on both sides of unistructure closed-end flattened tubes 26, using well-known ceramic techniques, eliminating the need for seals, such as those used in tubular stacks. [S. C. Singhal, *Proc. 6th Intl. Symp. Solid Oxide Fuel Cells*, Ed. By S. C. Singhal and M. Dokiya (Electrochemical Society, Pennington, N.J. 1999), p. 39.] On the other hand, the present invention provides the high power-to-volume ratios of planar stacks.

As described above, the SOFC stacking of this invention includes patterned layers. As would be understood by those skilled in the art, patterning can be performed during deposition and, as a result, no additional process steps are required. In particular, masking is readily incorporated and used with sputter deposition. Colloidal spray deposition processes are also contemplated in conjunction with contact masks, especially ultrasonic sprays which produce very small (20-40 μm) droplets. [A. Q. Pham, T. H. Lee, and R. S. Glass, *Proc. 6th*

Intl. Symp. Solid Oxide Fuel Cells, Ed. By S. C. Singhal and M. Dokiya (Electrochemical Society, Pennington, N.J. 1999), p. 172.] The design, assembly and resulting configuration of this invention provides several distinct advantages:

1. Improved mechanical strength and toughness. The devices are deposited onto an electrically insulating ceramic that can be chosen for desired strength, toughness, thermal conductivity, and thermal expansion match to cell components. Partially-stabilized zirconia is a preferred choice based on, its high toughness [T. Yoshida, T. Hoshina, I. Mukaizawa, and S. Sakurada, *J. Electrochemical Society*, 146, 2604 (1989)] and good thermal expansion match. Other materials with lower electrical conductivity and higher thermal conductivity may also be advantageous.
2. Simplified gas manifolding and sealing. The stacking geometry shown in FIG. 1 would require seals like other planar stacks. However, a flattened tube design allows simple gas manifolding as in various tubular stacks of the prior art. [S. C. Singhal, *Proc. 6th Intl. Symp. Solid Oxide Fuel Cells*, Ed. By S. C. Singhal and M. Dokiya (Electrochemical Society, Pennington, N.J., 1999).] That is, one gas is introduced through a feed tube into the closed-end flattened tube, and the other is fed to the outside. No sealing is required, or a single seal at the tube end can be used.
3. Small volume and weight. The design eliminates the separate interconnect pieces present in most planar stacks, and at the same time reduces the number of gas-flow channels by a factor of two. These changes reduce the volume and weight required to generate a given amount of power.
4. Reduced internal electrical losses. The integrated stack features intimate contact of electrodes with interconnects, eliminating the resistance loss associated with the pressure contacts used in many planar stacks. [B. Krogh, M. Brustad, M. Dahle, J. L. Eilertsen, and R. Edegard, *Proceedings of the 5th International Symposium on Solid Oxide Fuel Cells*, Ed. By U. Stimming, S. C. Singhal, H. Tagawa, and W. Lehnert, (Electrochemical Society, Pennington, 1997) p. 1234.] While pressure contacts to both ends of the integrated stack elements are required for current collection, the subdivision of the cell area into a large number of small series-connected cells results in relatively low currents and high voltages, such that losses at these contacts are minimal. Compare, for example, a 10 cm \times 10 cm single cell with the same size integrated stack element. (See, FIG. 8.) Assuming a single cell producing 0.5 W/cm 2 at an operating voltage of 0.7V, the total current is 70 A. On the other hand, the same area integrated stack with 45 2-mm-wide cells and 0.2-mm-wide interconnects will run at 22.5 V and ≈ 2 A. Assuming 2-mm-wide current collector strips at either end of the integrated stack, the collector current density would be the same as for a conventional cell. Thus, an $\approx 1\text{ }\Omega\text{cm}^2$ contact resistance would yield $\approx 0.5\text{V}$ drop at the contact: this would roughly halve the power density from the single cell, but would have negligible effect on the integrated stack.
- Another consideration is the lateral resistance loss across the electrodes. The resistance loss is given by $\rho L^2/2t_e$, where ρ is the electrode resistivity, L is the length of the current path (i.e. the cell width), and t_e is the electrode thickness. This relationship clearly shows that small cell widths minimize ohmic losses. For example, a LSM cathode ($\rho \approx 10^{-2}\text{ }\Omega\text{cm}$) with $L=2\text{ mm}$ and $t_e=20\text{ }\mu\text{m}$ yields $0.1\text{ }\Omega\text{-cm}^2$. This value is reasonably low even for this very thin electrode, and can be reduced further by reducing the cell width or increasing thickness. (See, FIG. 9.)
5. The unit cell size is very small in one direction, $\approx 2\text{ mm}$, and is several cm in the other. Scaleup of the stacks would involve primarily increasing tube length and number of cells,

and perhaps a slight widening of the tubes, such that there would be little change in the unit cell size. This will be very favorable in the scaleup stage of stack development, compared with conventional planar stacks where the individual cell area must be increased.

6. This invention provides considerable flexibility in stack design. For example, stack performance can be optimized by varying individual cell widths along the gas flow direction. The variation would be used to compensate for variations in gas composition and cell temperature along the length of the tubes. [See, for example, H. Yakabe, T. Ogiwara, I. Yasuda, and M. Hishinuma, *Proc. 6th Intl. Symp. Solid Oxide Fuel Cells*, Ed. by S. C. Singhal and M. Dokiya (Electrochemical Society, Pennington, N.J. 1999), p. 1087.] For example, since a lower-temperature region would likely have lower current densities, the cell widths would be increased slightly to retain the same current per cell.

As mentioned above, the present invention includes fabrication and/or methods for the construction and assembly of the stacking geometries and configurations described herein. As a point of contrast and comparison, consider techniques of the prior art: a tubular version of series-interconnected cells, where individual cells and interconnects were deposited in bands around calcia-stabilized zirconia (CSZ) support tubes. A major difficulty was obtaining patterned deposits with methods such as thick-film slurry coating and electrochemical vapor deposition (EVD). For example, a Ni—YSZ layer was slurry coated, then patterned by chemical etching. Electrolyte and interconnect layers were patterned by first covering selected areas with a loosely-bound powder, depositing the coating, and then mechanically scraping away the powder and the attached thick-film deposit. Disadvantages of these methods include the difficulty in scaling them into reliable mass production steps, the poor spatial resolution that led to relatively large unit cell sizes (1 cm), and the cycling to high temperature ($\approx 1500^\circ\text{C}$.) required for each deposition step.

Techniques recently developed for preparing low-to-medium temperature SOFCs, which typically involve thin (5-10 μm) electrolytes, are ideally suited for and can be readily applied to making the components, composites and stacks of this invention. Thin electrolytes and electrodes have been prepared using various colloidal deposition and sintering processes, [K. Z. Fung, J. Chen, C. Tanner, and A. V. Virkar, *Proc. 4th Intl. Symp. Solid Oxide Fuel Cells*, Ed. by M. Dokiya, O. Yamamoto, H. Tagawa, and S. C. Singhal (Electrochemical Society, Pennington, 1995) p. 676. S. deSouza, J. S. Visco and L. C. DeJonghe, *Solid State Ionics*, 98, 57 (1997)]. Tape calendaring and sintering, and sputter deposition methods are also well-known, reported in the pertinent literature and can be used to prepare such components. FIG. 12, for example, shows a cross-sectional SEM image of a typical sputter-deposited cell of the type available through prior art fabrication and now applicable to this invention, where the YSZ electrolyte and Ni—YSZ electrode were sputter deposited using such techniques. It is well known that sputter deposition can produce patterned thin films by depositing through shadow masks. Similarly, some of the colloidal processes such as spray deposition also can be used for patterned deposition.

Shadow masking is a simple technique for making patterned deposits. Mechanisms for accurately aligning shadow masks over planar substrates are readily available. As discussed above, it is desirable to have relatively small width cells. Feature sizes down to 0.1 mm are easily achieved, such that relatively small (e.g. 1-2 mm wide) cells can be prepared. Using the patterning techniques employed for banded-tubular SOFCs, it was more difficult to achieve the desired size reduc-

tion; 1-cm wide cells were used in those stacks, but this size does not provide the low ohmic loss observed with the present invention.

Cell component materials in the integrated stacks, geometries and configurations of this invention can be largely the same as those used in conventional SOFCs: YSZ electrolyte, LSM cathode, and Ni—YSZ anode. The same type of variations used to improve performance, e.g. addition of YSZ to the LSM cathode or ceria to the anode, can be employed, such variations including those discussed elsewhere herein. The interconnect material can be doped LaCrO_3 (LSC). As the interconnect conductivity required in an inventive stack is much lower than in conventional stacks (the interconnect layer is only several microns thick), alternate materials with lower conductivity than LSC can be used. Reference is made to Example 13 and FIG. 11.

An important aspect of an integrated stack is the support material. In prior work on the tubular banded cells, the support was calcia-stabilized zirconia, providing the advantage of excellent thermal expansion match with the YSZ electrolyte and other cell materials. However, the ionic conductivity was a problem because it tended to shunt the cells. In response thereto, another feature of this invention, distinct from the banded-tubular prior art, is low operating temperature, which minimizes support shunting. Another “problem” with zirconia is the poor thermal conductivity, which limits thermal shock resistance. Accordingly, support components of this invention can comprise materials overcoming such concerns, including but not limited to MgO and PSZ, partially-stabilized zirconia.

As mentioned above, the present invention could be used in any fuel cell application, including the full range of commercial applications which can be expected of fuel cells. A particular application of this stacking approach is for making small fuel cell power supplies for portable applications, especially those incorporating the low temperature cells of the type described elsewhere herein.

EXAMPLES OF THE INVENTION

The following non-limiting examples, data and referenced graphics illustrate various aspects and futures relating to the cell apparatus, assemblies, configurations and methods of this invention, including the surprising and unexpected results showing utility of hydrocarbon fuels at low temperature without carbon deposition. Comparable utilities and advantages can be realized using other embodiments, consistent with this invention. For instance, while numerous examples illustrate this invention through use of methane and ethane, other hydrocarbons including the corresponding alcohols can be used with equal effect through straight-forward modifications of this invention and related fuel cell components, such modifications as would be well known to those skilled in the art and made aware of this invention.

The SOFCs used in several examples were fabricated using techniques well-known in the art. In particular, several embodiments were utilized, but comparable results are available using other such electrodes and electrolytes, including those described herein. In some preferred embodiments for use with several examples, SOFCs were fabricated on porous $\text{La}_{0.8}\text{Sr}_{0.2}\text{MnO}_3$ (LSM) cathodes. The LSM pellets were ≈ 2 cm in diameter and 1 mm thick, and were produced using standard ceramic processing techniques. All SOFC layers, starting with a 0.5 μm -thick $(\text{Y}_2\text{O}_3)_{0.15}(\text{CeO}_2)_{0.85}$ (YDC) porous film, were deposited on the LSM pellet using dc reactive magnetron sputtering. The electrolyte, 8 mol % Y_2O_3 -stabilized ZrO_2 (YSZ), was subsequently deposited

15

under conditions yielding a dense 8 μm thick film. To complete the cell, another 0.5 μm -thick YDC film was deposited, followed by a porous, 2 μm -thick Ni—YSZ anode.

Anode reactions were studied using impedance spectroscopy with anodes that were sputter deposited onto both sides of bulk YSZ single-crystal electrolytes. Data was collected in various fuel environments at the indicated temperatures.

Example 1

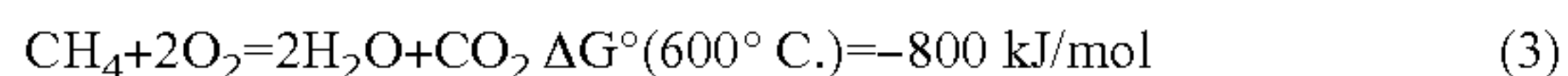
Single-cell current-voltage measurements were carried out in air and methane. Identical results were obtained for pure and humidified (containing 3% H_2O) methane in the early stages of cell tests; while cell performance was stable with dry methane, after ≈ 2 hrs of testing in humidified methane, cell performance degraded because of oxidation of the anode Ni. FIG. 1 shows the measured current density and power density vs. voltage. The open-circuit voltage (OCV) was 1.06V. The current density vs. voltage curves were non-ohmic indicating a substantial electrode overpotential. Based on prior studies of these cells operated on hydrogen fuel, the current densities were limited primarily by cathode, overpotential. Current densities increased with increasing temperature, such that maximum power density increased from 250 mW/cm^2 at 600° C. to 370 mW/cm^2 at 650° C.

Example 2

By way of comparison, the results of Example 1 were similar to those obtained for cells operated with humidified hydrogen fuel, except that the power densities were $\approx 20\%$ greater. Visual observation, energy dispersive x-ray (EDX), and scanning electron microscopy (SEM) observations of the anodes, carried out after the cell tests, showed no evidence of carbon deposition after ≈ 100 hrs of operation.

Example 3

Successful cell operation on dry methane (Example 1) indicated that direct electrochemical oxidation,



was the primary anode reaction mechanism. The OCV values measured in Example 1, $\approx 1.06\text{V}$, were typically very close to the values measured for these cells operated with 97% $\text{H}_2 + 3\%$ H_2O fuel. This is reasonable given that the $\Delta G^\circ(600^\circ \text{C.})$ values are similar for eqn. 3 and hydrogen oxidation. The exact Nernst potential for eqn. 3 cannot be calculated since the, H_2O and CO_2 partial pressures are not known, but the measured OCV_s suggest reasonable values, < 0.18 atm for H_2O and < 0.09 atm. CO_2 .

While eqn. 3 shows electrochemical oxidation of methane, it should be noted that the present invention contemplates the possibility of other reaction mechanisms for the desired oxidation products. For instance, various intermediate reactions and/or species can exist enroute to complete oxidation under cell operating conditions. While eqn. 3 illustrates methane oxidation, equations can be provided to portray oxidation of other hydrocarbons discussed herein, likewise accounting for and including the presence of various other intermediate reaction mechanisms and/or species.

Example 4

It is unlikely that hydrocarbon reforming played a role in the cell operation of Example 1, and if so, only after H_2O and CO_2 were produced by reaction (3). Discounting such an occurrence, reforming rates were probably too low to contribute significantly to the anode reaction, because of the

16

small anode area ($\approx 1 \text{ cm}^2$) and low temperature. Furthermore, the relatively high fuel flow rates used invariably flush any reformation reactants and products from the anode compartment.

Example 5

Direct hydrocarbon oxidation is further evidenced by impedance spectra (FIG. 2) obtained from the above-described Ni—YSZ/YDC anodes in humidified methane (a) and humidified dilute H_2 (b). An 3% $\text{H}_2 + 3\%$ $\text{H}_2\text{O} + 94\%$ Ar mixture, which was used to simulate a slightly reformed methane fuel (b), yielded electrode arcs with a much different shape than those for methane, indicating that the primary anode reaction with methane was not oxidation of hydrogen produced by reforming. Also shown in FIG. 2 is the impedance result for the anode operated in 97% $\text{H}_2 + 3\%$ H_2O (c). This electrode arc was much smaller than that for methane, indicating a lower anode overpotential and explaining why the SOFC current densities were higher for hydrogen than methane.

Example 6

It is thought that one factor contributing to the rapid direct electrochemical oxidation of methane at these temperatures is the anodes employed in the SOFCs and, in particular a combination of Ni—YSZ and YDC layers. This is illustrated in FIG. 3, which compares the impedance spectra taken in humidified methane for Ni—YSZ/YDC and Ni—YSZ anodes. The YDC layer causes a factor of ≈ 6 decrease in the electrode resistance. This observation is consistent with prior studies indicating that ceria promotes hydrocarbon oxidation. Without restriction to any one theory or mode of operation, ceria is believed to be beneficial for several reasons. First, it becomes a mixed conductor in a reducing fuel environment, a condition which should expand the reaction zone beyond three-phase boundaries. Second, the ionic conductivity of ceria is higher than that of YSZ, which improves the transport of oxygen ions from the electrolyte to the anodes. Third, ceria is known to readily store and transfer oxygen. The present invention also indicates that the oxygen storage capability of ceria can be enhanced by the addition of zirconia. Preferred embodiments include anodes with two ceria/zirconia interfaces where enhanced oxygen storage can, in this manner, increase methane/hydrocarbon oxidation rates.

Example 7

Another result observed from the cell tests of this invention was the absence of carbon deposition. In general, carbon deposition can occur by methane pyrolysis,



or disproportionation,



On the other hand, the oxygen flux arriving at the anode during SOFC operation tends to react with any carbon, suppressing carbon deposition. The role of methane pyrolysis was tested by flowing pure methane over SOFC anodes, without SOFC operation, such that no reaction products were present. No carbon deposition was observed at $< 700^\circ \text{C.}$, and the amount of carbon deposited increased only with increasing temperature above 700°C. , showing carbon deposition via methane pyrolysis does not occur readily at low temperatures.

17

Example 8

During cell operation, product gases are present in the anode compartment, raising, at least, the possibility of carbon deposition via reaction (5). However, as noted above, the present cell tests provide data for nearly pure hydrocarbon in the anode compartment, perhaps due to the small-area cells and relatively high fuel flow rates resulting in small concentrations of reaction products. Even so, consideration was given to the situation encountered in a SOFC stack, where the products of reactions (1)-(3) would be present at substantial partial pressures. Thus, a simple equilibrium calculation was done to determine the conditions where one might expect carbon deposition free stack operation in CO—CO₂ mixtures. FIG. 4 shows the CO/CO₂ partial pressure ratio at equilibrium with graphitic carbon (eqn. 5) vs. temperature, for two CO+CO₂ total pressures. For sufficiently low CO/CO₂ ratios, carbon deposition will not occur. The optimal temperature range for SOFC stack operation on dry methane is 500-700° C. If the temperature is <500° C., carbon deposition proceeds by reaction (5) unless CO/CO₂ ratios are very low. While temperatures \geq 700° C. would tend to suppress carbon deposition by reaction (5), they would allow carbon deposition by direct pyrolysis of methane (eqn. 4).

Example 9

Some internal reforming would be necessary in a SOFC stack to produce a small amount of CO and H₂. However, carbon monoxide and hydrogen gas would balance the CO₂ and H₂O produced by direct oxidation, preventing exceedingly low CO/CO₂ and H₂/H₂O ratios where the anode Ni may oxidize.

Example 10

Ethane fuel reactions were studied in SOFC's with anodes of low Ni content. Various cells were made using Ni—YDC anodes containing 10, 20 and 40 weight percent Ni. The porous Ni—YDC anodes were \approx 2 μ m-thick. The cell structure and processing was similar to that described above, except that the cathode was an LSM-YSZ mixture. In order to identify carbon-free operating conditions, the Ni—YDC anodes were tested in ethane fuel environments at temperatures ranging from 500-700° C.

Ethane oxidation was studied at Ni—YDC anodes using low Ni concentrations intended to limit carbon deposition. FIG. 5 summarizes carbon deposition results at the various Ni—YDC anodes exposed to dry and wet (3% H₂O) ethane from 500-600° C. These reaction studies were made without cell operation and indicate the onset of carbon deposition for the given conditions. In wet ethane, anodes with lower Ni content (10-20 wt %) were more resistant to carbon deposition at higher temperatures. For dry ethane fuel, carbon deposition occurred even for low temperatures and anodes with low Ni content. These observations show that carbon-deposition-free cell operation can be conducted using wet ethane with any of the above anode compositions at 500° C., and up to 550° C. for anodes with 10-20 wt % Ni.

Example 11

Current voltage measurements of cells were taken under operating conditions that avoided carbon deposition. The performance of a cell operating with wet (3% H₂O) ethane fuel at 500° C. (\blacktriangledown) is illustrated in FIG. 6 and compared to wet hydrogen 92% hydrogen (\bullet) and humidified dilute (94% Ar)

18

hydrogen (\blacksquare). In this case the Ni—YDC anode contained 40 wt % Ni. The cell current densities were relatively low because of the low temperature. Current densities for ethane fuel were typically about 35% less than for hydrogen fuel. A maximum of \approx 35 mW/cm² was obtained with ethane. No carbon deposition was detected. Carbon-deposition-free cell operation with anodes of lower Ni content (10-20 wt %) was achieved up to 600° C., which is beyond the temperature range indicated by the carbon reaction studies given in FIG. 5. This suggests that the oxygen flux arriving at the anode during cell operation reacted with any carbon, thereby suppressing carbon deposition. However, cell power densities were somewhat low in these cells, either because of low anode electrical conductivity or low Ni catalyst content.

Example 12

With reference to FIGS. 7A and 7B, the solid oxide fuel cell components of this invention can be stacked as shown in FIG. 10. Flattened support tubes allow high volume densities and minimize sealing problems. The integrated configurations eliminate interconnects and reduce the number of flow fields by two, relative to planar fuel cells of the prior art. Because the integrated arrays are not in contact, heat conductors can be inserted therebetween; this can help eliminate thermal gradients and improve efficiency through reduction of cooling requirements. Current flows along the surfaces of the fuel cell rather than between separate components thereof.

Example 13

With reference to FIGS. 7A, 7B and 10, the fuel cell components and material composition thereof can be selected according to performance and function parameters desired. FIG. 11 provides construction profiles of two such fuel cells of this invention, as designed according to desired/relative operating temperatures. Such cells, in accordance with the broader aspects of this invention, can be integrated as described herein and incorporated into an assembly of such cells. Various other material choices and component constructions would be well-known to those skilled in the art and made aware of this invention, depending upon a particular performance property or parameter desired. Such designs and constructions are limited only by the availability of a desired component material to be used in conjunction with thin layer fabrication techniques.

Example 14

Current procedures can involve first depositing anode material, followed by electrolyte. After high temperature sintering, interconnect and cathode layers are applied and sintered at a lower temperature. Thin Ni—YSZ anodes and YSZ electrolytes are deposited using a colloidal processing technique called centrifugal casting. In this method, a partially-sintered Ca-stabilized Zirconia (CSZ) ceramic pellet (the support for the ISOFC) is immersed in a slurry, based on water or acetone, that contains the appropriate powder. Patternning is achieved simply by placing an adhesive polymer mask on the pellet. The pellet and slurry are then placed in a centrifuge where centrifugal forces are used to rapidly deposit the powder onto the pellet surface, yielding high quality, high packing density Ni—YSZ or YSZ coatings. The layers and support are co-sintered in air at 1400-1500° C. FIG. 13 shows an optical microscope image of a patterned Ni—YSZ strip after sintering. The layer is uniform with a low-defect-density and well-defined patterned edges.

Example 15

A key issue in the processing of example 14 is the drying stress caused by the liquid evaporating from the thin Ni—YSZ and YSZ layers. The film shrinkage during drying can cause cracking, and is generally worse for thicker films and smaller particle sizes. The process described herein uses nano-scale YSZ for the electrolyte to reduce sintering temperatures. It produced several micron thick YSZ films in single step. Multiple deposition steps were used to make thicker layers. Another aspect of this process is co-sintering. Fuel cells require a thin dense YSZ layer with porous cathodes, anodes, and support. Difficulties can include matching shrinkages (to avoid cracking of the layers and/or sample curvature) and maintaining electrode porosity at the high temperatures required for YSZ sintering.

High temperature sintering at 1500° C. resulted in high quality dense YSZ electrolytes. An SEM image of the top surface of atypical YSZ layer is shown in FIG. 14. The YSZ layer is clearly dense and defect free, with a large grain size. The shrinkages were matched well: no cracking or curvature of the samples was observed. FIG. 15 shows a SEM image of a portion of a patterned YSZ film. The YSZ film is seen in one region while the other region while the uncovered Ni—YSZ

preferred electrolyte YSZ ($CTE \approx 10.5 \times 10^{-6} \text{ K}^{-1}$). As mentioned above, a useful material is partially-stabilized zirconia (PSZ), which has an excellent thermal expansion match with YSZ. The partial stabilization results in transformation toughening and also results in a substantially lower ionic conductivity than fully stabilized zirconia. In the experiments described below, PSZ processing was developed to produce high strength supports with reasonable porosity, and the effect of the electrical conductivity on shunting the SOFCs was estimated.

Example 18

Ceramic supports were fabricated using standard ceramic processing techniques, i.e. calcining the as-purchased powder to vary particle size, thoroughly dry-mixing the powder with pore former, uniaxially pressing the mixture into pellets, and finally sintering. Archimedes density measurements and scanning electron microscopy were used to analyze the porosity and structure of the supports. In order to investigate the factors that most affect substrate porosity and strength, an experiment was designed using the D-Optimal method, which attempts to pick the trials that will give the most information based on the parameters in the experiment. The factors and levels used in the study are listed below in Table 1.

TABLE 1

Factors and levels examined in the substrate porosity study			
Factor	Level 1	Level 2	Level 3
Material	Partially Stabilized Zirconia (PSZ, 3 mol % Y_2O_3 , Tosoh TZ-3YS)	Yttria Stabilized Zirconia (YSZ, 8 mol % Y_2O_3 , Tosoh TZ-8YS)	PSZ with 20 wt % Al_2O_3 (PSZ-A, Tosoh TZ-3Y20A)
Calcining Time (hr)	2	3	4
Calcining Temperature (Celsius)	900	1000	1100
Filler (starch) amount (wt %)	5	10	15

anode can be seen in another region. This result, along with that shown in FIG. 13, demonstrates successful fabrication of patterned anode and electrolyte layers.

Example 16

The successful fabrication of a patterned anode and electrolyte on a support can be challenging aspects of this type of ISOFC processing. Additional steps involve simple slurry painting and relatively low temperature sintering, using techniques well-known to those in the art.

An ISOFC of this invention can, preferably, have a ceramic interconnect, such as $LaCrO_3$. However, an Ag paste can also be used as the interconnect for purposes of illustration. Above $\approx 600^\circ \text{C}$., this material sinters to a high density, providing a good gas seal. It is easily painted onto an ISOFC. A cathode typically comprises standard SOFC materials: (La, Sr) MnO_3 (LSM) or (La,Sr) (Co,Fe) O_3 (LSCF), as can be applied by painting followed by relatively low temperature sintering.

Example 17

Desireable properties for a fuel cell support include (1) high resistivity, (2) high strength and toughness, (3) a stable porous structure at the operating temperature, (4) low cost, and (5) a thermal expansion coefficient matching that of a

Powders (all from Tosoh) were mixed with appropriate filler (starch) and uniaxially pressed into four 1-inch diameter pellets. The filler was burned out at 400° C. for 2 hours with a ramp rate of 5° C. per minute. The samples were then sintered at 1200° C. for 6 hours with a ramp rate of 10° C. per minute. Half of the pellets were set aside for mechanical testing, while the other half were sintered at 1400° C. for 6 hours to simulate the high temperature conditions that would be used in fuel cell fabrication. One of the high temperature samples was used to measure porosity by the Archimedes method, using water as the fluid. The biaxial flexural strength of all the samples was determined using the Ball-on-Ring method. [G. de With and H. Wagemans, "Ball-on-Ring Test Revisted," *J. Am. Ceram. Soc.*, 72 [8] 1538-41 (1989).] Multiple regression analysis was used to formulate models for porosity and flexural strength in terms of the factors studied.

Example 19

In order to investigate the effects of current shunting by the porous PSZ support, 2-point conductivity measurements were performed on round PSZ pellets with about 30 vol % porosity and a thickness of about 1.5 mm. Electrical contacts were made by painting silver squares on the flat sides of the pellets and attaching silver wires (see FIG. 16). Resistance was read directly from the two contacts.

21

Example 20a

Notwithstanding other anode materials of this invention, the anodes of this example were of NiO (Baker) and YSZ (Tosoh) in a 70:30 weight ratio, translating to roughly 55 vol % Ni in the reduced state. The material was sintered at 1200° C. for 6 hours after screen printing. The cathodes were either of 1) $\text{La}_{0.6}\text{Sr}_{0.4}\text{Fe}_{0.8}\text{Co}_{0.2}\text{O}_3$ (LSFC) and Gadolinium-doped Ceria (GDC) in a 1:1 weight ratio, which were sintered at 900° C. for 3 hours after screen printing, or 2) $\text{La}_{0.8}\text{Sr}_{0.2}\text{MnO}_3$ (LSM) and YSZ in a 1:1 weight ratio, which were sintered at 1200° C. for one hour. All prints were made with inks formed by mixing the above powders with Heraeus vehicles, of ethyl cellulose and terpeneol.

Example 20b

For the four-cell stacks described below (FIG. 20), two different fabrication or processing procedures were used. First, the anode (Ni—YSZ), electrolyte (YSZ), and interconnect ($\text{La}_{0.65}\text{Sr}_{0.2}\text{Ca}_{0.15}\text{CrO}_3$) were printed in that order, with a drying step after each layer, then subsequently co-fired at 1400° C. for 6 hours. The cathode was then printed, dried, and the stack was sintered under the conditions described above. The images shown below are for ISOFCs prepared in this way. Illustrating a second fabrication method, the Ni—YSZ anode was screen printed, followed by centrifugal casting of YSZ (described below) and co-firing at 1400° C. for 6 hours. The Ag interconnect and LSCF-GDC cathode were then screen printed and fired at 900° C. for 3 hrs.

Example 20c

Two-point electrical conductivity was measured for screen-printed anodes and cathodes. Silver contacts were made to both ends of the anode strip, which was printed on a porous PSZ substrate (FIG. 17).

Example 21

The YSZ slurry, referenced in the preceeding example, was prepared from 1 gram of YSZ powder (Tosoh) mixed with 200 ml ethanol and sonicated for 1 hour to get a stable suspension or slurry.

PSZ substrates were placed in a vessel with a flat bottom and 10 mL of the slurry added along with 10 mL of ethanol. The vessels were then placed in a centrifuge with a radius of 20 cm for 30 min at 1500 rpm. In the centrifugal field, the ceramic particles in the suspension are forced down to the surface of the substrate to form a coating—the supernatant was clear after the centrifuge process. After decanting the supernatant, the wet green body was allowed to dry. The coated pellets were dried in open air for more than 8 hours, and then sintered 1400° C. for 4 hours.

Example 22

A representative three-dimensional plot of the flexural strength (MPa) versus filler (wt. percent) and material (PSZ to YSZ to PSZ-alumina) shows that PSZ generally has the highest strength, followed by PSZ-alumina and finally YSZ. As expected, higher filler content results in lower strength due to increased porosity. A strength plot holding material and filler content constant, shows a very slight decrease in strength with increasing calcining time and an apparent maximum with calcining at 1000° C. Plotting the porosity at a calcining temperature and time of 1000° C. and 2 hours, respectively, shows a general increase in porosity with increasing filler content, as expected. PSZ and PSZ-alumina show overall

22

higher porosity than YSZ. Holding the material (PSZ) and filler content (15 wt %) constant shows very weak dependence of porosity on calcining time and temperature; the variations in porosity shown are easily attributable to error associated with the Archimedes method. Comparing such data, it is clear that the material and filler amount most affect the substrate strength and porosity. Based on all the data, a useful substrate formula for development of the ISOFC comprises PSZ calcined for 2 hours at 1000° C. with 15 wt % of added filler. (Note that linear shrinkages remained essentially constant at $\approx 20\%$ in all cases examined.)

Example 23

One issue with PSZ supports is their ionic conductivity, which can lead to a shunting of the ISOFC stack current, with decreasing cell voltage and efficiency. Initial studies were done to estimate this leakage current using the following assumptions:

- 10 cm \times 10 cm ISOFC, 10% of cell area for interconnect
- 45 2-mm-wide cells
- 0.5 W/cm² at 0.7 V (1.4 A, 31.5 V)

Leakage currents calculated using the stack voltage and substrate resistance (derived from the substrate conductivity and dimensions) are listed below in Table 2. Overall, the expected leakage currents are fairly small, <4% of cell current at 800° C. and <1% at 600° C., showing cell performance not greatly affected by the PSZ substrate.

TABLE 2

Porous PSZ substrate conductivity and calculated leakage currents at various temperatures			
T	600° C.	700° C.	800° C.
Conductivity (S/cm)	6.25×10^{-4}	2.03×10^{-3}	5.32×10^{-3}
Leakage current	0.006 A (0.42%)	0.02 A (1.4%)	0.05 A (3.6%)

Example 24

The ISOFC structures, designs and geometries of this invention are best employed with electrodes having sufficient conductivity to transport current across each cell without significant loss. If one assumes a 0.6 Ωcm^2 cell resistance (electrolyte ohmic loss and electrode polarization resistances) and 0.2 cm² cell area (2 mm wide, 10 mm long), one obtains an individual cell resistance of 30 Ω . Assuming that a preferred anode should contribute no more than one tenth of that measured resistance, its resistance should be 0.3 Ω , which translates into a sheet resistance of 1.5 Ω/square .

Anode sheet resistances measured as shown in FIG. 17 are presented in FIG. 18, which shows that a Ni—YSZ anode sheet resistance was well below 1.5 Ω/square . Given that the electrode thickness was $\approx 10 \mu\text{m}$, the Ni—YSZ conductivity was $\approx 1 \times 10^3 \text{ S/cm}$ in the 500° C.-800° C. temperature range, in agreement with literature values. [N. Q. Minh, "Ceramic Fuel Cells," *J. Am. Ceram. Soc.*, 76 [3] 563-88 (1993).]

Example 25

The measured sheet resistances for cathodes consisting of $\text{La}_{0.6}\text{Sr}_{0.4}\text{Fe}_{0.8}\text{Co}_{0.2}\text{O}_3$ (LSFC) and Gadolinium-doped Ceria (GDC) in a 1:1 weight ratio, shown in FIG. 19, are much higher than the desired 1.5 Ω/square . The resistivity calcu-

23

lated for the thickness of $\approx 10 \mu\text{m}$ at 800°C . is $0.4 \Omega\text{cm}$. The relatively high resistivity is presumably due to the high GDC content in the electrode; prior studies have shown that adding 50% of a poor conductor generally decreases the conductivity at least 10 times. A relatively thick over-layer of pure LSFC, on top of the LSCF-GDC, serves to increase cathode conductivity. $(\text{La,Sr})\text{MnO}_3$ is expected to yield similar results.

Example 26

As noted above, screen printing is a preferred fabrication technique for the present array of SOFC's 12 and corresponding structure and geometry because of its low cost (relative to technologies such as electrochemical vapor deposition and sputter deposition), its ability to produce patterns with $50 \mu\text{m}$ lateral resolution, and because all ISOFC layers can be deposited using this method. The processing scheme was as follows. First, anode 18 was deposited, followed by electrolyte layer 20 and interconnect 22. Second, these layers and support 14 were all co-sintered at 1400°C . Third, cathode layer 16 was deposited. Fourth, the cathode was sintered.

FIG. 20 shows schematically, in cross-section, the screen printed layers and patterns resulting from the deposition sequence described above.

FIG. 21 shows a cross-sectional SEM image of an ISOFC, such as that described above, printed on a porous PSZ substrate. The fired layer thicknesses are about $10 \mu\text{m}$ and the cathode and anode are visibly porous. The YSZ electrolyte is fairly dense with only a small amount of closed porosity visible in the sample. Furthermore, the substrate shows an open pore network, which allows gas transport to the electrode. There were no catastrophic film failures (e.g. peeling or cracking) observed, so the shrinkages of the substrate and layers are in close proximity of one another. There was, however, some slight sample curvature perhaps due to differential sintering. The ISOFC processing and fabrication of this example shows that the desired patterning accuracy was achieved, and each component shows the desired structure.

Example 27

Four-cell ISOFC tests on devices similar to those shown in FIGS. 20 and 21 were prepared and tested. Centrifugal casting, as described above, was used to deposit the electrolyte, and Ag ink was used for the interconnect. Patterning of the centrifugally cast electrolyte layers was achieved by using masks of adhesive tape during the centrifuge process. Silver wires were attached to the end anode and cathode current collectors. Voltage versus current and power were measured with air as the oxidant and humidified hydrogen as the fuel, using a standard single cell test configuration. The results of the test at different temperatures, given in FIG. 22, showed a maximum stack voltage of 3.2V, somewhat lower than the expected value of 4.4V (1.1V per cell). Stack current and power increased with increasing temperature, as expected for solid oxide fuel cells. The maximum power was $\approx 25 \text{ mW}$ at 700°C . This relatively low value is presumably due to insufficient conductivity of the cathode layers in this demonstration stack—this was expected since the LSCF-GDC cathode conductivity is not very high. This value is low relative to single thin-electrolyte SOFCs with similar materials, but note that such tests are usually made with additional Pt mesh current collectors to minimize resistance losses. Extra current collectors were not used in the present test. It will be relatively easy to improve on the results in FIG. 15 can be improved by adding pure LSCF layers on top of the LSCF-GDC to decrease the sheet resistance.

24

Example 28

With reference to FIGS. 7A and 23, an array of solid oxide fuel cells 12, connected in series by thin-film interconnects 22, can be deposited about, and/or top and bottom, a closed-ended tubular porous, insulating support 14, as can be fabricated using partially-stabilized zirconia, as would be understood by those skilled in the art and made aware of this invention. The components of layer 12 can be deposited, as described elsewhere herein, on opposed sides of flattened tubular support 14. With reference to tubular stacks of the prior art, such a configuration/geometry further reduces sealing requirements, with improved overall performance.

Consistent with the preceding summary, detailed description, figures and data, the following examples provide results on the fabrication and performance of planar patterned series-connected SOFCs with smaller cell widths (e.g., about 1 to about 2 mm) and lower operating temperature, as compared to the prior art. Such widths are small enough to minimize electrode resistance losses even for relatively thin layers, while still being large enough to fabricate using low-cost methods such as screen printing. In addition, small widths provide relatively high voltages in small devices, important for portable applications of SOFCs. FIGS. 7A and 20, for instance, show a cross sectional schematic view of four-cell arrays. Relatively thin ($\approx 10\text{-}40 \mu\text{m}$) electrolytes were used to allow operating temperatures less than about 800°C . The foregoing and several of the following examples briefly describe the methods used to achieve PSZ support porosity and mechanical strength. The screen printing of anode, electrolyte, interconnect, and cathode layers, along with their electrical properties and microstructure, are also described.

Example 29

With reference to examples 17-18, partially stabilized zirconia $((\text{ZrO}_2)_{0.97}(\text{Y}_2\text{O}_3)_{0.03}$, PSZ) was chosen as one support material candidate based on its excellent coefficient of thermal expansion (CTE) match ($\text{CTE} \approx 10.5 \times 10^{-6} \text{ K}^{-1}$) with fully stabilized zirconia $((\text{ZrO}_2)_{0.92}(\text{Y}_2\text{O}_3)_{0.08}$, YSZ) and the other cell materials. A low (3 mol %) yttria content lowers the material cost, decreases the ionic conductivity, and increases the mechanical strength relative to YSZ. PSZ is also chemically compatible with the Ni—YSZ anode and YSZ electrolyte. One drawback of PSZ is its ionic conductivity, which will tend to shunt the array current. PSZ tends to degrade in humid environments between $100\text{-}400^\circ\text{C}$., but this is below the SOFC operating temperature range.

In order to investigate the factors that most affect substrate porosity and strength, an experiment was designed using the computer program EDO (Version 1.0, Nextbridge Software), which uses the D-Optimal method to pick the trials that will give the most information based on the parameters in the experiment. The three materials chosen for the study were YSZ, PSZ, and PSZ-A (PSZ with 20 wt % Al_2O_3), all from Tosoh. The zirconia-based powders were calcined at 900 , 1000 , or 1100°C . for 2, 3, or 4 hours, and 5, 10, or 15 wt % starch pore former was added. The powders were uniaxially pressed into pellets (2.5 cm diameter, 2 g each) at a die pressure of $\approx 175 \text{ MPa}$. The pellets were fired first at 400°C . for 2 hours with a ramp rate of 5°C . per minute to burn out the starch. The temperature was then increased at 10°C . per minute to 1200°C . and held for 6 hours. Finally, sintering was carried out at 1400°C . for 6 hours. Porosity was determined by the Archimedes method, using water as the fluid, while biaxial flexural strength was determined using the Ball-on-Ring method.

25

Example 30

With reference to example 26, screen printing was chosen for fabrication of array component layers because it is a simple, inexpensive, widely-used method that can produce patterns with the required lateral resolution (<0.1 mm). Screen printing inks were made by mixing powders with a vehicle, Heraeus V-737, which consists mainly of ethyl cellulose and terpineol. Anode inks were prepared from NiO (J. T. Baker) and YSZ (Tosoh) powders mixed in a 70:30 weight ratio, translating to ≈ 55 vol % Ni in the reduced state. Electrolyte inks were made with YSZ powder (Tosoh). Interconnects were made using commercial Au ink (Heraeus). The cathode inks consisted of $\text{La}_{0.6}\text{Sr}_{0.4}\text{Fe}_{0.8}\text{Co}_{0.2}\text{O}_3$ (LSCF, Praxair) and $\text{Ce}_{0.9}\text{Gd}_{0.1}\text{O}_2$ (GDC, NexTech) in a 1:1 weight ratio, or pure LSCF.

Prints were made using a standard screen printer. After printing, the layers were dried at 150°C . for 30 minutes. The anode and electrolyte were deposited first, followed by co-sintering of the anode, electrolyte, and support at 1400°C . The cathode layer was printed and sintered at 900 - 950°C . for 3 hours. Finally, the interconnect layer was printed. The interconnect was not sintered except during heating for cell testing. In some cases, sufficient curvature developed during high-temperature sintering to prevent further screen printing; for these cells the interconnect and cathode layers were hand-painted using the same inks. Also, in some cases the cathode layer was applied after the interconnect layer.

Example 31

Models for substrate porosity and flexural strength were formulated using a multiple regression software tool (Multiple Correlation Analysis, Version 4.01). Table 3 lists calculated biaxial flexural strengths and porosities for the various materials at 5 and 15 wt % starch. Calcining temperature and time had very little effect on porosity and strength, so in the calculation they were kept constant at 1000°C . and 2 hr., respectively. Experimental data generally fell within the ranges calculated by the models. From these results, it was evident that PSZ's strength was >2 times that of YSZ and PSZ-A. At 15 wt % starch, PSZ had a strength of 140-160 MPa, whereas YSZ and PSZ-A were both in the range of 60-80 MPa. Higher filler content resulted in lower strength due to increased porosity. For example, the model showed that increasing filler content from 5 to 15 wt % would decrease PSZ strength by nearly a factor of 2. Similar, but less dramatic, effects were observed for YSZ and PSZ-A. Linear shrinkages were 20% in all cases.

TABLE 3

Material	Wt % starch	Biaxial Flexural Strength (MPa)	Porosity (vol %)
PSZ-A	5	100-120	15-20
	15	60-80	30-35
YSZ	5	120-140	5-10
	15	60-80	25-35
YSZ	5	280-300	0-5
	15	140-160	25-30

The following conditions produced desirable properties and were thus chosen for subsequent fabrication: a filler content of 15 wt % in PSZ calcined for 2 hours at 1000°C ., yielding a strength of ≈ 130 MPa and a porosity of ≈ 30 vol %. It was subsequently found that the calcining step could be eliminated without significantly changing the properties, and many of the results described below were with supports made without calcining.

26

Example 32a

As discussed above, in the preceding description and elsewhere, a series-connected design or configuration of this invention can include electrodes that have sufficiently low sheet resistance R_s to transport current across each cell without significant loss. A target area-specific resistance (ASR) contribution from an electrode, <0.05 Ωcm^2 , is obtained by requiring that each electrode ohmic loss be $<\approx 10\%$ of the stack resistance, and assuming a 0.5 Ωcm^2 cell ASR (electrolyte ohmic loss and electrode polarization resistances). Using a standard expression for electrode resistance, $\text{ASR} = R_s L^2 / 2$, where L is the electrode width of 0.1 cm, $R_s < \approx 10$ Ω/square is obtained. Given the above numbers, the maximum power density for the array would be ≈ 0.5 W/cm^2 , calculated based on the active cell area. Note that increasing L to 0.2 cm decreases the desired R_s to $<\approx 2.5$ Ω/square .

Example 32b

With reference to example 20c, two-point resistance measurements were carried out on screen-printed Ni—YSZ layers. The sheet resistance of single Ni—YSZ layers, presented in FIG. 24, was 0.2 - 0.25 Ω/square from 500°C .- 800°C ., well below the desired value of 10 Ω/square . Thus, single Ni—YSZ printed layers should provide negligible contribution to the array resistance. Given the single-print thickness of ≈ 10 μm , the Ni—YSZ conductivity was ≈ 1000 S/cm, in fairly good agreement with literature values.

Example 33

FIG. 25 summarizes screen-printed cathode sheet resistance measurements. LSCF-GDC alone had a high R_s value of ≈ 2000 Ω/square at 800°C .; this is not surprising given the 50 wt % content of low-conductivity GDC. While a composite layer is desirable because of its good electrochemical performance, only the portion within ≈ 10 μm of the electrolyte appears to contribute significantly to the electrochemical processes. Thus, multiple prints were made consisting of an initial LSCF-GDC layer followed by one or more layers of pure LSCF. Each layer was ≈ 15 μm thick. As shown in FIG. 25, adding one layer of LSCF significantly reduced R_s to ≈ 25 Ω/square at 800°C . Two and three layers of pure LSCF further reduced R_s to ≈ 8 and 5 Ω/square at 800°C ., respectively. Thus, two or more layers of LSCF yielded the desired $R_s < 10$ Ω/square .

Example 34

With reference to example 20b and related discussion, FIG. 26 shows fracture cross-sectional SEM micrographs from a typical four-cell array, along with a portion of the support, taken after cell testing. The low magnification image shows that the PSZ support had porosity striations, the result of the starch pore-former added during processing. The Ni—YSZ layer was ≈ 15 μm thick, and was porous with an average particle size of ≈ 1 μm . The YSZ layer was a double print, reasonably dense with mostly closed porosity, and ≈ 40 μm thick. This result, together with the cell test result below, demonstrate that screen printing and co-sintering can be used to produce reasonably dense patterned YSZ electrolytes. Thinner electrolytes may be desired, however, and can be achieved by adjusting the screen type, ink, printing conditions, or using a single print. The cathode bi-layer was ≈ 30 μm thick with a porous structure (≈ 0.5 μm particle size), good adhesion to the electrolyte, and no clear evidence of the interface between the LSCF-GDC and LSCF layers. The Au interconnect in this array (not shown in the figure) showed

limited porosity, presumably because its sintering temperature was at the maximum cell test temperature of 800° C. Nonetheless, it had sufficient density to produce reasonable performance as discussed below and elsewhere herein.

Example 35a

Cell tests were carried out by sealing the PSZ supports to alumina tubes using Ag ink, and contacting Ag leads to the interconnect pads at each end of the four-cell array using Au ink. The test was carried out with air at the cathode and humidified hydrogen fed through the tube to the anode. The individual cells had active areas, defined by the area of anode-cathode overlap, of 0.9 cm×0.1 cm, or ≈0.09 cm². The results of a four-cell array test, for the structure shown in FIG. 26, are given in FIG. 27. (See also, comparable results in FIG. 22 and example 28.) The open circuit voltage (OCV) ranged from 3.22-3.55 V, well below the theoretical value of ≈4.4 V. A shunting current in the PSZ support may be partly responsible for the low OCV. Slight porosity in the electrolyte and interconnect layers may also be responsible-note that single cells with screen printed YSZ electrolytes showed maximum OCV values of only 0.9-1.0V.

Example 35b

No diffusion limit was observed at high currents, indicating that the support had sufficient porosity. The maximum power density was ≈140 mW/cm² at 700° C. and ≈220 mW/cm² at 800° C. These power densities are substantially less than observed for anode-supported cells with these materials, ≈500 mW/cm² at 700° C. and ≈1000 mW/cm² at 800° C. The low power densities are believed due in large part to the low OCV values, 0.8-0.9 V per cell; for example, the stack ASR was only 0.8 Ωcm² per cell at 800° C., which would yield a maximum power density of 375 mW/cm² if the OCV were 1.1 V. The two-layer cathode sheet resistance of 25 Ω/square was larger than the desired 10 Ω/square, contributing 0.1 Ωcm² to the stack resistance. The relatively thick YSZ electrolyte ASR was ≈0.1 Ωcm² at 800° C. The strong temperature dependence and non-linear shape of the current-voltage curves suggest a substantial electrode polarization contribution, especially at lower T. Thus, improving electrolyte and interconnect density, decreasing electrolyte thickness, increasing the cathode thickness, and improving the electrode structure should all improve power density.

As provided by the preceding discussion, millimeter-scale series-connected SOFC arrays have been fabricated and tested. Optimization of the substrate processing, structure, and strength were carried out, and screen printing inks and printing conditions were developed to achieve desired component structures. Screen printing was shown to be a useful method for fabricating all the patterned layers. Electrical testing of four-cell arrays was carried out, and while reasonable power densities were obtained, higher values can be achieved by increasing OCV values via improved electrolyte and interconnect density, decreasing cathode sheet resistance, decreasing electrolyte thickness, and decreasing electrode polarization losses.

While the principles of this invention have been described in connection with specific embodiments, it should be understood clearly that these descriptions, along with the chosen figures, charts, graphics, and data therein, are made only by way of example and are not intended to limit the scope of this invention, in any manner. For example, the inventive anodes and related cellular components have been shown as utilized with various hydrocarbons; however, as would be well-known to those skilled in the art and made aware of this invention, the methods described herein can also be utilized with various other higher molecular weight hydrocarbon

stocks or reaction systems. Likewise, while certain ceria and/or electrolyte materials have been described herein, others can be used alone or in combination and with or without various dopants to achieve the same or similar effect. While various parameters, such as temperature and concentrations, have been described in conjunction with the construction, fabrication and/or operation of various fuel cells and their components, the same parameters can be varied in order to achieve oxidation rates and/or power densities comparable to those described herein. Other advantages and features of this invention will become apparent on the following claims, with the scope thereof determined by the reasonable equivalents, as would be understood by those skilled in the art.

We claim:

1. A solid oxide fuel cell assembly, comprising:
 - a substantially planar array of fuel cells on a substrate support, each said cell comprising cathode, anode, electrolyte and electrode interconnect component structures, said substrate support having a thermal expansion coefficient match with said electrolyte, each said component structure of each said cell in a substantially planar arrangement of said each component structures; and
 - a fuel cavity across said planar electrode arrangements, said assembly providing reduced resistance to current flow with increased cell number.
2. The assembly of claim 1 wherein each said fuel cell has a width dimension ranging from about 0.1 mm to about 2 mm.
3. The assembly of claim 2 wherein said dimension is about 0.1 mm.
4. The assembly of claim 1 wherein at least one of said cathode and said anode have a thickness dimension of about 10 μm.
5. The assembly of claim 4 wherein said cathode comprises LSM.
6. The assembly of claim 4 wherein said anode comprises Ni—YSZ.
7. The assembly of claim 6 wherein said electrolyte comprises YSZ.
8. The assembly of claim 1 where said substrate support comprises a PSZ.
9. A method of using reduced operating temperature to reduce current shunting loss from a solid oxide fuel cell, said method comprising:
 - providing a substantially planar array of fuel cells on an ionically-conducting substrate support, each said cell having a width dimension and comprising cathode, anode, electrolyte and electrode interconnect component structures, each said component structure of each said cell in a substantially planar arrangement of said component structures; and
 - operating said array of cells at a temperature less than about 800° C.
10. The method of claim 9 wherein said ionic substrate support comprises a PSZ.
11. The method of claim 9 providing increased voltage across said cells with reduced cell width.
12. The method of claim 11 wherein each said fuel cell has a width dimension of about 2 mm.
13. The method of claim 12 wherein said substrate support comprises a PSZ.
14. The method of claim 13 wherein said operating temperature is between about 600° C. and about 800° C.
15. The method of claim 14 wherein said cell dimension is about 0.1 mm.

UNITED STATES PATENT AND TRADEMARK OFFICE
CERTIFICATE OF CORRECTION

PATENT NO. : 7,709,124 B2
APPLICATION NO. : 10/427707
DATED : May 4, 2010
INVENTOR(S) : Barnett et al.

Page 1 of 1

It is certified that error appears in the above-identified patent and that said Letters Patent is hereby corrected as shown below:

Column 1, Lines 11-13:

“The United States government has certain rights to this invention pursuant to Grant No. DE-G626-00NT40814 from the Department of Energy to Northwestern University.” should read
--This invention was made with government support under DE-FG26-00NT40814 awarded by the Department of Energy. The government has certain rights in the invention.--

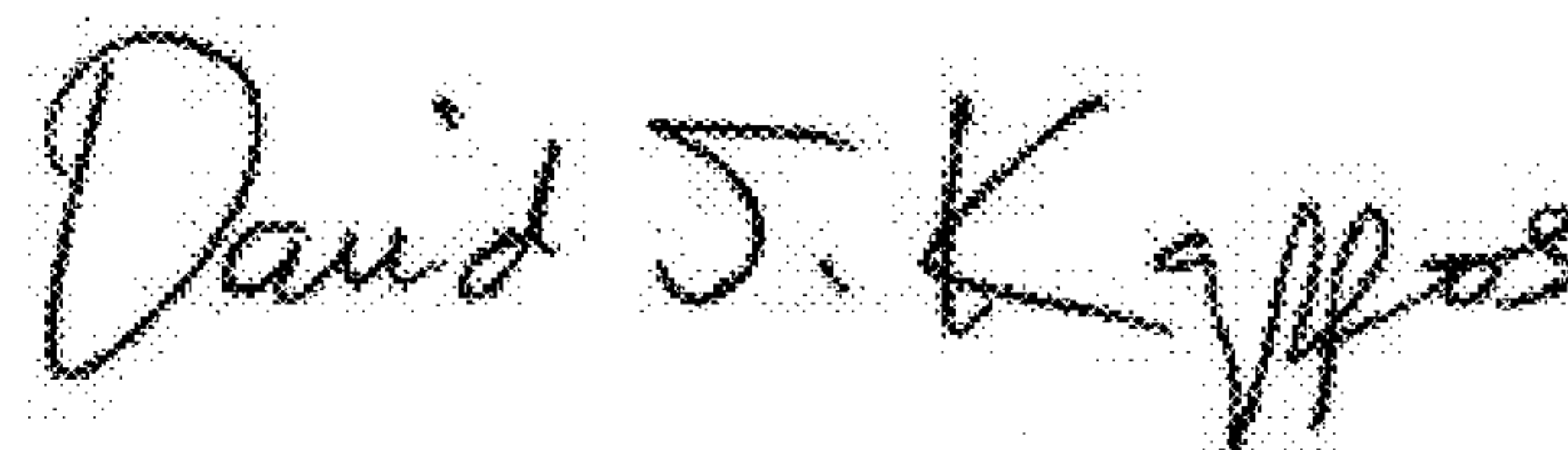
Column 12, Line 10:

“on,” should read --on--

Column 17, Line 66:

“(▼)” should read --(▲)--

Signed and Sealed this
Eleventh Day of October, 2011

A handwritten signature in black ink, reading "David J. Kappos". The signature is written in a cursive, flowing style with a large initial "D".

David J. Kappos
Director of the United States Patent and Trademark Office